

Scaling in the global spreading patterns of pandemic Influenza A (H1N1) and the role of control: empirical statistics and modeling

Xiao-Pu Han^{1,2}, Bing-Hong Wang^{1,3}, Changsong Zhou^{2,4,*}, Tao Zhou^{1,5}, Jun-Fang Zhu¹

1 Department of Modern Physics, University of Science and Technology of China, Hefei 230026 China

2 Department of Physics, Hong Kong Baptist University, Hong Kong

3 The Research Center for Complex System Science, University of Shanghai for Science and Technology and Shanghai Academy of System Science, Shanghai, 200093 China

4 Centre for Nonlinear Studies, and The Beijing-Hong Kong-Singapore Joint Centre for Nonlinear and Complex Systems (Hong Kong), Hong Kong

5 Web Sciences Center, University of Electronic Science and Technology of China, Chengdu 610054, China

* E-mail: Corresponding author: cszhou@hkbu.edu.hk

Abstract

Background: The pandemic of influenza A (H1N1) is a serious on-going global public crisis. Understanding its spreading dynamics is of fundamental importance for both public health and scientific researches. Recent studies have focused mainly on evaluation and prediction of on-going spreading, which strongly depends on detailed information about the structure of social contacts, human traveling patterns and biological activity of virus, etc.

Methodology/Principal Findings: In this work we analyzed the distributions of confirmed cases of influenza A (H1N1) in different levels and find the Zipf's law and Heaps' law. Similar scaling properties were also observed for severe acute respiratory syndrome (SARS) and bird cases of H5N1. We also found a hierarchical spreading pattern from countries with larger population and GDP to countries with smaller ones. We proposed a model that considers generic control effects on both the local growth and transregional transmission, without the need of the above mentioned detailed information. We studied in detail the impact of control effects and heterogeneity on the spreading dynamics in the model and showed that they are responsible for the scaling and hierarchical spreading properties observed in empirical data.

Conclusions/Significance: Our analysis and modeling showed that although strict control measures for interregional travelers could delay the outbreak in the regions without local cases, the focus should be turned to local prevention after the outbreak of local cases. Target control on a few regions with the largest number of active interregional travelers can efficiently prevent the spreading. This work provided not only a deeper understanding of the generic mechanisms underlying the spread of infectious diseases, but also some practical guidelines for decision makers to adopt suitable control strategies.

Introduction

A new global influenza pandemic has broken out. In the first three months, the epidemic spreaded to over 130 countries, and more than 10^5 people were infected by the novel virus influenza A (H1N1). H1N1 represents a very serious threat due to cross-species transmissibility and the risk of mutation to new virus with increased transmissibility. Several early studies paid attention to this public issue from different perspectives [1–8], and made known important information such as the biological activity of H1N1 virus and the patterns of early spreading. While every effort was taken to develop antiviral and vaccination drugs, efficient reduction of the spreading could have already been achieved by interventions of population contact. However, such interventions, like strict physical checking at the borders and enforced quarantine,

are costly and highly controversial. It is therefore difficult to decide the control strategies: when should the schools be suspended and whether the border control should be reinforced or given up?

The detailed mechanism of transmission can differ significantly for different virus, the spreading patterns, however, may display common regularities due to generic contacting processes and control schemes. Many health organizations have collected large amount of information about the spreading of H1N1. In-depth analysis of these data, together with what we have known for SARS [9,10], avian influenza (H5N1) [11,12], foot-and-mouth epidemic [13,14] and some other pandemic influenza [15,16], may lead us to a more comprehensive understanding of the common spreading patterns that do not rely on the detailed biological features of virus. In this paper, we studied the spreading patterns of influenza pandemic by both empirical analysis and modeling. Our main contributions were threefold: (i) The Zipf's law of the distribution of confirmed cases in different regions were observed in the spreading of H1N1, SARS and H5N1; (ii) A simple model was proposed, which does not rely on the biological details but can reproduce the observed scaling properties; (iii) The significant effects of control strategies were highlighted: the strong control for interregional travel is responsible for the Zipf's law and can sharply delay the outbreak in the regions without local cases, while the focus should be turned to local prevention after the outbreak of local cases. Our analysis provided a deeper understanding of the relationship between control and spreading, which is very meaningful for decision makers.

Results

Empirical Results

We first analyzed the *cumulative* number n_i of laboratory confirmed cases of H1N1 of each country i to a given date (see the data description in *Materials and Methods*). Because n_i is growing, the distributions for different dates are normalized by the global total cases $N_T = \sum n_i$ to the corresponding dates for comparison. What we used in our analysis is the Zipf's plots [17], which was obtained by sorting each $n_i > 0$ in a descending order, from rank 1 to the largest value M and plotting n_i with respect to the rank r_i . We considered the normalized Zipf's plot where each n_i was replaced by its corresponding proportion $P_i = n_i/N_T$. More discussion of the Zipf's plot can be found in *Materials and Methods*. Table 1 shows the ranking of the top 20 countries and their total of confirmed cases in five typical dates. Fig.1(a) and 1(b) report the Zipf's plots for the distributions of normalized n_i in different dates. The maximal rank M corresponds to the number of regions with confirmed cases, which grows during the spreading. The normalized distributions P surprisingly display scaling properties. Before the middle of May, P shows clearly a power-law type $P \sim r^{-\alpha}$ with an exponent α changing around 3.0 (except the first data point, see Fig. 1(a)). Although the total cases N_T grows rapidly in this early stage, P for different dates seems to follow the same line in the log-log plot. After the middle of May, the middle part of the distribution grows more quickly, and meanwhile the virus spreads quickly to many more countries. In this stage the exponent α of the left part of P steadily reduces from higher than 3.0 to 1.7 (see Fig. S3(b) in *Supporting Information*), and an exponential tail emerges (Fig. 1(b)). After June 10, P can be well fitted by a power-law function with an exponential tail, for example, $P \sim r^{-1.70}e^{-0.013r}$ for the data of July 6 (solid line, Fig. 1 (b)). The scaling properties are not special for H1N1, but quite common in various diseases, such as SARS in 2003 (Fig. 1(c), $\alpha \approx 2.7$) and the bird cases of H5N1 in 2008 (Fig. 1(d), $\alpha \approx 2.0$), although the spreading range is much more limited (to only about 30 countries).

There could be variations or errors in the real-world surveillance of H1N1, which may affect the ranking of the countries. To examine the robustness of our analysis against such variations, we considered several types of possible variation: (A) the variation is correlated with the reported total of cases in a country; (B) the variation is correlated with the population of the country; and (C) the variation is correlated with both the reported total of cases and the population of the country. We found that the form of power-law-like distribution in Zipf's plot is robust under these different types of variations (Fig. S1). This

analysis shows that our finding of the power-law-like form is still believable in the presence of variations or errors in surveillance. The detailed discussion can be found in the *Supporting Information*.

Another scaling property which is often accompanied by Zipf's law is the Heaps' law [6, 19, 20]. Heaps' law describes a sublinear growth of the number of distinct sets $M(t)$ as the increasing of the total number of elements $N_T(t)$ belonging to those sets, with the power-law form $M \sim N_T^\lambda$. A detailed introduction can be found in *Materials and Methods*. In the pandemic of H1N1, the number of infected countries M and the global total confirmed cases N_T obeys the Heaps' law with the Heaps' exponent $\lambda \approx 0.35$ before May 18, 2009 and $\lambda \approx 0.53$ after May 18 (Fig. 2). The exponents of the Zipf's law and the Heaps law satisfy $\alpha\lambda \approx 1$, which is consistent with the theoretical analysis [21] that if an evolving system has a stable Zipf's exponent, its growth must obey the Heaps' law with exponent $\lambda \approx 1/\alpha$ (an approximate estimation when $\alpha > 1$: the larger the α , the more accurate the estimation). After May 18, the pronounced exponential tail in the distribution P (Fig. 1(b)) leads to a deviation from strict Zipf's law, and the two exponents no longer satisfy the relationship $\lambda \approx 1/\alpha$.

We also found that broad distribution of n_i is related to heterogeneity in different countries. Figs. 3(a) and 3(b) report the dependence between the number of confirmed cases n_i and the population and gross domestic product (GDP). A clearly hierarchical spreading pattern, similar to what were predicted by some theoretical complex network models [22, 23], can be observed: the big and rich countries were infected first, and then the disease spread out to the global world. This can be understood that bigger and richer countries usually have more active population in international travel, and thus are of higher risk to be new spreading origins in the early stage of epidemic. The evolution of correlations between the confirmed cases n_i and population and GDP was reported in Fig. 3(c) by the *Kendall's Tau* τ_K . Kendall's Tau measures the correlations between two datasets which are strongly heterogeneous in magnitude. The method to calculate τ_K was introduced in *Materials and Methods*. To test whether τ_K is significant, we compared the value from original datasets to those from surrogate data by shuffling the order of the population of GDP (see *Supporting Information*). Significantly positive correlations with a tendency of increase with time can be observed (Fig. 3(c) and Fig. S2). These results show that the interconnectivity among world regions and human mobility are important factors that accelerate the spread of diseases globally. The global total confirmed cases N_T displays two phases of growth (Fig. 3(d)): in the early stage N_T increases with a high rate and then turns into a stable exponential growth with a much smaller rate, with the transition occurring around the middle of May. Such a transition may reflect the changes in the contacting rate among people due to imposed or self-adaptive control.

It is interesting to study whether and how the exponent α in the distribution P is related to the well-known reproductive number R in mathematical epidemic theory. Employing the method in Ref. [1] and the estimate of the mean serial interval of 3.2 days in Ref. [2, 3], we estimated, using the growth rate in the stable growth period after the middle of May, that R is between 1.09 and 1.22 for the serial interval in the range [1.9, 4.5] days. This range is slightly smaller than the results in several other estimations based on the early spreading [4, 5], but generally in agreement with other studies based on the spreading after the early outbreak [3]. As seen in Fig. S3(a) in *Supporting Information*, there is a rapid decrease of R in the period before the middle of May. As we will show later in the model, the decrease of R could be attributed to the control effects. Interestingly, the power-law exponent α of the distribution P has a similar trend of evolution (Fig. S3(b)). A positive correlations can be found in the plot R vs. α for the early stage when both of them are relative large. This relationship could be explained as follows. In the early stage of spreading, R is effectively higher when surveillance and control schemes for H1N1 were not very effective. On the other hand, only a small portion of the population was infected. In this stage, local growth was quicker than transmission between countries, so that the reported number decreases quickly with rank, corresponding to a larger α . However, a simple relationship between R and α is not expected because α from the normalized distribution of a given date is related to the accumulated effects of R before this date, especially in the later stage of spreading.

We also investigated the statistical regularities within a country. We compared the normalized dis-

tribution of confirmed cases in different states of USA and in different provinces of China (Fig. 4): P of USA shows a much more homogeneous form with a large deviation from strict power-law distribution while P of China is close to a power-law with exponent $\alpha = 1.79 \pm 0.04$ (the Zipf's distribution of SARS cases of different provinces of China is also a power-law type with exponent $\alpha \approx 3$ [28]).

We have investigated the growth of the number of confirmed cases n_i for all the 13 countries with $n_i > 10^3$ until July 6, and found that the patterns are quite diverse. As shown in Fig. 5, some have a clear transition in the middle of May from a rapid breakout to a stably exponential growth (e.g. U.S.A. and Mexico), which is similar to the global growth patterns; some have much later initial infections (e.g. Australia); some exhibit a stably exponential growth without a pronounced crossover (e.g. China); and some show irregular growth curves (e.g. Japan and New Zealand). The spreading of H1N1 was impacted by many factors, such as control measures, traffic systems, school terms, and so on, which could lead to such diverse growth patterns under a stable global growth.

To summarize, the empirical results show that the scaling properties in epidemic spreading process may widely exist at different regional levels and crossing various infectious diseases. In the following we tried to obtain some insight into the generic mechanisms underlying these common properties.

Modeling and Simulation Results

The empirical results provoke some outstanding questions: how to understand the scaling properties in region distributions, which factors lead to the different spreading patterns for different regions, and what are the effects of control measures on the regional level spreading? We believed that the scaling properties have the origin at the generic contact process underlying the transmission of diseases, and the variation could result from the heterogeneity of the contact process in different diseases and regions. One most important heterogeneity may be the control strength. To build a generic model incorporating the effects of control, let us consider the actions taken by people when facing a serious epidemic spreading. In general, individual people try to take many approaches to reduce the probability of infection, such as using respirator, reducing the face-to-face social interactions, and disinfecting frequently. Meanwhile, many organizations usually take measures to prevent the spreading of epidemic, such as physical examinations in public transportation and schools, isolation for highly risky groups, and so on. If epidemic breaks out in a country, other countries may reinforce the health examinations at the borders for the travelers from that country. For example, in China, measurement of body temperature was used in many airports and border crossings, and the identified infected persons and their close contacts were strictly isolated in the early stage of H1N1 spreading. In Hong Kong, students had to measure body temperature and were not allowed to go to school when the temperature was higher than a threshold. These actions of individuals and social organizations can effectively change the structure of social contacts, reduce infection probability and affect the spreading patterns of epidemic [29,30]. Such effect of imposed or self-adaptive controlling actions was the starting point of our model.

Different from many individual-based models, our model is in the regional level, so the detailed social contact structure [9,31,32,34,35] as well as the control methods and strategies in individual level [36–38] are not considered directly. Our scheme was based on the metapopulation framework. In this framework, the global community is divided into a set of regions, each having its own spreading dynamics, but also interacting with each other. This framework has been widely used in modeling epidemic spreading in the last decade [39–43]. In our model, a region (such as a country) is denoted by a node in a network with K nodes in total. Different from previous work considering details of transportation [9,44] or mobility [45] networks, the network is supposed to be fully-connected since in general there are direct contacts between almost all countries in the world. However, the strength of connections between countries could be different due to the heterogeneity in various factors, such as population and economics. As will be shown later, while such heterogeneity has some impact on the epidemic spreading, the most important ingredients are the strengths of control within and between regions. Therefore, instead of employing the detailed information of real traffics, we generically denoted the international traffic of a node as its

strength s_i , and the weight of link between two node i and j is assumed to be symmetric and proportional to the products of the strengths s_i and s_j :

$$q_{ij} = s_i s_j / \sum_{k=1}^K s_k. \quad (1)$$

The spreading at time t from node j to i is proportional to the number of infected cases n_j of node j , together with a time-varying effective weight $w_{ij}(t)$ of the link, namely $w_{ij}(t)n_j(t)$. Here $w_{ij}(t)$ is related not only to the link strength q_{ij} , but also to the control strategy. Control measures are in general reinforced on the travelers from countries with large number of infected cases, and thus in our model the link weight is

$$w_{ij}(t) = q_{ij} n_j(t)^{-\beta_1}, \quad (2)$$

where β_1 is a free parameter. Effectively, we can take $w_{ij}(t) = 0$ if $n_j(t) = 0$. Note that while q_{ij} is symmetric, w_{ij} is in general asymmetric. This expression describes generically the effects of various control measures at the borders, without relying on the details at the individual level.

In this model, the update of the number of cases n_i of an arbitrary node i consists of two parts: a local infection growth and the global traveling infections:

$$\Delta n_i = \rho \left[a_i(t) n_i(t) + \frac{b}{\langle s \rangle} \sum_{j=1, j \neq i}^K w_{ij}(t) n_j(t) \right], \quad (3)$$

where ρ is a positive constant related to the basic transmissibility of the diseases, $\langle s \rangle$, the average value of s_i , is introduced for normalization, and the coefficient b denotes the relative contribution due to the transmission from other regions. Note that Δn is generally a real number while the real-world increment of infected cases must be integral. Therefore, we round Δn to the neighboring integer, namely to set $n_i(t+1) = n_i(t) + [\Delta n] + 1$ with probability p and $n_i(t+1) = n_i(t) + [\Delta n]$ with probability $1 - p$, where $p = \Delta n - [\Delta n]$ ($[x]$ denotes the largest integer no larger than x).

The relative contribution by local infections, $a_i(t)$, is not constant, but reflects the strength of control within a region. In the same vein as the border control in Eq. 2, we described the generic effects of local control by decaying $a_i(t)$ as a function of n_i with a free parameter β_2 , namely

$$a_i(t) = \begin{cases} n_i(t)^{-\beta_2}, & \text{if } n_i(t)^{-\beta_2} > g \\ g, & \text{if } n_i(t)^{-\beta_2} \leq g. \end{cases} \quad (4)$$

Effectively, $a_i(t) = 0$ if $n_i = 0$. Here the decaying of a_i is limited by a constant g ($0 < g < 1$), which accounts for the necessary social contacts in the daily life even under the outbreak of the epidemic. In reality, g is also related to the transmissibility and death rate of the disease.

In our model, n_i is the total infected cases of a node. In reality, the reported and confirmed cases are most likely a small part of the total cases. If we assume that the ratio of reported cases is similar for different countries and roughly constant in time, the model can be used to describe the distribution of confirmed cases without changing our conclusions in the following.

To focus on the effects of the control parameters β_1 and β_2 , we first considered the simplest case in which s_i is uniform. In this case, $q_{ij} = 1/K$ and Eq. (3) is reduced to the minimal model

$$\Delta n_i = \rho \left[a_i(t) n_i(t) + \frac{b}{K} \sum_{j=1, j \neq i}^K n_j(t)^{1-\beta_1} \right]. \quad (5)$$

The impact of the heterogeneity in s_i will be discussed later.

We would like to emphasize that the effect of control considered in our model does not refer in particular to any of the specific control measures. Eqs. (2) and (4) are supposed to describe generically the integrated effects of various intervention schemes, either imposed by governmental policies or self-organized by individuals. For example, the border control parameter β_1 describes the integrated effect

of all the measures impacting on the spreading across different countries, and β_2 not only includes the impact of some official control measures, but also the impact of some adaptive individual actions, such as reducing of social contact, and wearing gauze mask. All of our discussions of "control" are based on this extended meaning.

In the following, to represent a worldwide network of countries, the total number of nodes in our model is $K = 220$. The model can also be used to represent the spreading within a county when regarding a node as a region within a country and ignoring the transmission from other countries. From Eq. (3), the parameter ρ does not affect the pattern of the normalized distribution P . ρ is thus fixed at 0.2 in all our simulations, which is close to the fast growing rate of the influenza A in the early stage of outbreak (see Fig. 3(d)). We quantified the epidemic spreading initiated randomly at one node by the spreading range M (the number of nodes with $n_i > 0$) and the total cases N_T and investigate how they depend on the control parameters β_1 and β_2 (Fig. 6). It is seen that both large β_1 and large β_2 can reduce the range of spreading M , but the control on the interregional borders by β_1 is more effective than β_2 (Fig. 6(a)). On the contrary, large β_2 is much more effective than β_1 to reduce the total number of cases N_T (Fig. 6(b)). The patterns in Fig. 6 are generic in the model for different parameters ρ , b and g and for different time during the spreading. These results imply that once a country has local epidemic outbreaks, its growth will be mainly driven by the local spreading but not the input of foreign cases.

The parameter space of β_1 and β_2 can be divided into four regimes, corresponding to the combinations of weak or strong and local or interregional controls, as indicated in Fig. 6. Typical normalized distributions P obtained in the four regimes are compared in Fig. 7. When β_1 is small (regimes (I) and (II)), the epidemics can spread to almost all nodes in short time, and P is rather homogeneous. When β_1 is large (regimes (III) and (IV)), the spreading across different region is suppressed, and P is rather inhomogeneous, manifested as a power-law-like form. Keeping β_2 fixed, the exponent α clearly increases with β_1 and a larger β_2 can slightly increase α further (inset, Fig. 7(a)). We have included a detailed discussion of the time evolution of the distributions P and their association to the Heaps' law in Fig. S5 of the *Supporting Information*.

While β_1 has a sensitive impact on the interregional spreading and controls the heterogeneity of the distribution P , β_2 mainly affects the growth of total cases N_T , especially in the early stage (Fig. 7(b)). With stronger control at larger β_2 , the fast growth of N_T in the early stage will be effectively suppressed and transformed to a slow exponential growth within shorter time. As seen in Eq. (4), β_2 only affects the growth of the epidemic in the very early stage after it appears in a region. The significant effect of β_2 on the growth of total cases N_T emphasizes the importance of early epidemic control, in agreement with the conclusion of previous studies on other diseases [13, 14].

Comparing the results from the four regimes, we can see that the spreading pattern in regime III (large β_1 and small β_2) is closer to the empirical observations of influenza A. In this regime, the range of α covers most of empirical results. For example, with $\beta_1 = 0.8$ and $\beta_2 = 0.2$, the distribution P can be well fitted by a power-law function with exponent 1.67 (Fig. 7(a)), and this value is close to the empirical exponent of influenza A on July 6 (Fig. 1(b)). Large β_1 and small β_2 is consistent with the real-world situation. While more efficient to implement control measures on the borders, e.g., to identify infected and suspected candidates and their close contacts for quarantine, it is much more difficult to get the same efficiency for the same control schemes in local communities. The relative lower death rate of influenza A is also likely to weaken the self-adaptive control and voluntary isolation of the individuals, leading to insignificant change of the contact patterns (e.g., much weaker than SARS). All these will render a lower efficiency in the local control, corresponding to a small β_2 and a larger g .

Besides the two parameters β_1 and β_2 for the border and local control, the other two parameters b and g related to interregional and local contact rates can also significantly affect the spreading processes. The parameter b in our model denotes the relative strength of interregional transmission. Large flow of interregional travels can also make the epidemic spread to most of the regions rapidly. As a result, the distribution P becomes more homogeneous with decreasing α when b is larger; however, b has only a

slight impact on the growth pattern of N_T (Fig. 8(a)).

The parameter g expresses the background local growth speed which cannot be further reduced due to unavoidable social contacts even under the effect control measures. Under strong border control (large β_1), the number of infected cases n_i is mainly determined by g , growing exponentially with the rate ρg after an initial transient period, thus g has a very sensitive impact on the growth of the total number N_T (Fig. 8(b)). If g is large, earlier infected regions will have much more infected cases compared to later infected regions, leading to an inhomogeneous distribution P . At smaller g , the earlier and later infected regions do not differ very much in the number of infected cases, corresponding to more homogeneous distribution P with decreasing α (Fig. 8(b)). Different from the case of weak border control (small β_1), homogeneous P here does not mean the rapid spreading; on the contrary, it denotes the situation that the infection in each country is in a low level.

All the above discussions are based on the minimal model where the diversity of the nodes and the edges is ignored by assuming a uniform s_i . Now we study the impact of heterogeneous s_i and the effect of target control on the spreading of disease. While previous investigations have focused overwhelmingly on the impact of heterogeneity in the degree of complex networks [9, 22, 34, 35], here we study the effects of the heterogeneity in the intensity of nodes and links in globally coupled networks. We first took the real population of different countries as s_i in our model and investigate how does the initiation of the disease in countries with different ranks of populations influence the global spreading. When the disease starts in a country with a large s_i (Fig. 9(a), population rank $R_{ini} = 11$ as Mexico), the disease spreads out quickly and the spreading process displays a clear tendency from the node with large s_i to those with small s_i as seen by the evolution of the scatter plot of $n_i(t)$ vs. s_i and the Kendall's tau (Fig. 9(c)), which reproduces the main features in the empirical data in Fig. 3. On the contrary, when the initiation happens in a country with small population (Fig. 9(b), population rank $R_{ini} = 100$ as Libya), the disease is contained in the country where it is initiated for a period of time, and then the countries with the largest populations get infected soon and become new centers of spreading. τ_K is around zero in the very beginning when the diseases is contained and becomes negative when spreading to a few nodes with the largest s_i and quickly shift to positive values when the new centers take the leading role in the spreading (Fig. 9(c)). The total cases N_T grows much faster in the first case (Fig. 9(d)). We applied target control in our model (see *Material and Methods*), and we found that strong control just on one or two nodes with the largest s_i can sharply reduce the spreading by several orders of magnitude (Fig. 9(e)). This effect is similar to target immunization of the hubs in degree heterogeneous complex networks [36]. Here the results are shown for one realization of the simulation. The statistics over many realizations displayed in Fig. S6 in the *Supporting Information* can evidently demonstrate the spreading from the nodes with large s_i to those with small s_i . A more systematic analysis of the effects of node heterogeneity and target control by considering a power-law distribution of s_i is included in the *Supporting Information*. We find that even though the heterogeneity can accelerate the spreading (Fig. S7), the strength of control plays the leading role to determine the patterns of spreading (Fig. S8). The spreading can be sharply decelerated by reducing both the total cases N_T and range M , when only a few nodes with the largest s_i are in strong border control (Fig. S9).

Another extension of our model considers the diverse effects of control in different country to qualitatively explain the different growth patterns for different country shown in Fig. 5. We assume that the parameters β_1 and β_2 are nonidentical and are randomly chosen between 0 and 1 for different nodes, while we fix the other parameters. In reality, all the important parameters ρ , β_1 , β_2 , g , and b can be different due to variation of contact structures (population, hygiene condition, culture, etc.) from country to country. Here we did not intend to fit the model precisely to the real data, but rather to demonstrate the concept and to prove the principle.

The results were summarized in Fig. 10 for two groups of nodes with early and late initial infections. In each group, we consider four combinations of the parameters β_1 and β_2 . For the nodes where the disease is initiated and got infected in the very beginning (Fig. 10 (a)), the other nodes are not infected

and there is no significant input, thus the growth patterns are dominantly determined by β_2 . When β_2 is close to 1, the local growth rate shifts quickly to ρg , corresponding to an exponential function without a clear transition. A pronounced transition happens when β_2 is close to zero and it takes a period time for the local growth rate to settle down to ρg . The growth patterns of the late infected nodes depend on both β_1 and β_2 (Fig. 10(b)): the transition to stably exponential growth is still determined by β_2 , while larger β_1 prevents the input from other nodes and makes n_i smaller. In all the cases, the stable growth rates are close to ρg (the slope $\approx \rho g \log_{10} e$), therefore additional variation of ρg can account for diverse exponential growth rates in the data. We can see that the basic growth patterns in empirical data, i.e., with and without a pronounced transition, can be reproduced by different control parameters in the model. The model, however, does not include strong non-stationary ingredients that could lead to sudden increase of n_i observed in a few countries in Fig. 5.

Fig. 10 also shows the corresponding N_T in this model of diverse control parameters, which also reproduce the feature of N_T in the data. The behavior is similar if we further include the diversity in the parameter g . We would like to point out that the growth patterns of n_i in the individual nodes with different parameters are similar to various growth patterns of the global total N_T in the model without diversity in parameters. This provides justification that we can apply our model to the global level where each node represents a country, or to the level within a country where each node denotes a state/province. In the later case, N_T of the model represents the growth of the total cases of a country and is consistent with the growth of n_i in the former case when similar interregional parameters β_2 and g are considered in both level, namely the model at different level will provide consistent conclusion about the epidemic spreading.

To summarize, power-law distribution of P with large exponent α appears in situations with large β_1 , small b and large g . This regime corresponds to the real situations that the epidemic control for the travelers is strong, the interregional contact is much weaker compared to that in local communities, and the change of local social contacts by the disease is not very significant. The epidemic control for the interregional travelers (large β_1) is the most important condition for the emergence of the power-law type of P , since the power-law distribution cannot be generated when β_1 is close to zero no matter what other parameters are.

Discussion

The statistics of region distributions of several pandemic diseases, including H1N1, SARS and bird cases of H5N1 display obvious scaling properties in the spreading process at different levels. We studied the origin of such scaling properties with a model of epidemic spreading at the regional level that incorporates the generic effects of intervention and control measures without the need of the structure details of social contacts and the particularity of the transmission of the diseases. Such a model is then able to capture the general principles underlying epidemic spreading and to reveal the generic impact of control measures. We elucidated that strict epidemic control on interregional travellers plays an important role in the emergence of the scaling properties.

The results of the model can cover the empirical statistics of H1N1 on both the region distribution and the growth of total cases, and are also consistent with the region distributions of SARS and H5N1. In particular, the exponent α of the empirical distribution P of H1N1 is about 3.0 in the early stage and changes to 1.7 on July 6, 2009, and α is about 2.7 for SARS and 2.0 for H5N1. In the stable spreading period, the α of H1N1 is smaller than SARS and H5N1. According to the understanding from our model, larger α indicates that the control measures are more strict and effective. This is in agreement with the situation in SARS and H5N1 spreading. Because of high death rate and strong infection capability, SARS gave rise to strong social panic and attracted attentions from citizens to governments in the countries with outbreaks, such as China, and strict control measures were enforced in each public transportation systems and in daily life of people. As for H5N1, many efficient control measures were also taken to prevent the

spreading, such as immunity for poultry and culling of livestock, etc. Large α in the early stage of the spreading of H1N1 could be related to stronger control effect due to overrating of the mortality of H1N1. Empirical results also showed that the distribution P of H1N1 in USA is more homogeneous than in China. While there are probably several factors contributing to this difference, but the most obvious difference is in the control measures. China took strict control policies, such as entry screening at airports and border crossings, and enhanced surveillance of outpatients and inpatients with influenza-like illness, enforced quarantine and isolation for identified infected persons and the close contacts, which are not so strict compared to those during the SARS spreading, but are stronger than USA.

Our main findings, i.e., interregional control mainly affects the spreading range and the form of the region distributions while local control sensitively impacts the growth of total cases, provide us a picture of epidemic control. For regions that have no or only a few local infected persons, strict control measures for interregional travellers can delay the local outbreaks significantly, but if there are large number of local cases, these control methods for travellers are not so important. Instead, control methods and treatment for local communities will be much more helpful. After the Summer of 2009, the focal point of the control policies for H1N1 of many countries turned to the treatment for infected persons. According to the conclusions of the present model, this strategy shift is reasonable. This model also indicates that the diversity of different regions will accelerate the spreading. Efficient prevention of the spreading could be achieved by enhanced control measures, especially for the giant regions. Further work will be focusing on the impact of target [8] or voluntary vaccination [46].

In summary, a simple physical model basing on the abstraction of the generic contact processing and the effects of control can provide meaningful understanding of the scaling properties commonly observed in various pandemic diseases. It deepens our understanding of the relationship between the strength of control and the spreading process, and provides a meaningful guidance for the decision maker to adopt suitable control strategies.

Materials and Methods

0.1 Data Description

The cumulative number of laboratory confirmed cases of H1N1 of each country is available from the website of Epidemic and Pandemic Alert of World Health Organization (WHO) (<http://www.who.int/>), which started from April 26 to July 6, and updated each one or two days. Each update is in a new webpage, for example, the data in May 21 is shown in the webpage (http://www.who.int/csr/don/2009_05_21/en/index.html). After July 6, WHO stopped the update for each country since the global pandemic has broken out.

Table 1 lists the countries with the rank of confirmed cases up to 20 in several typical dates. The corresponding total of confirmed cases is shown after the country name in the table. A complete list of the data in these typical dates can be found in *Supporting Information*.

The data for SARS and H5N1 are respectively available from the websites of WHO (<http://www.who.int/csr/sars/country/en/index.html>) and the World Organization for Animal Health (OIE) (<http://www.oie.int/wahis/public.php?page=disease>) respectively. The data for H1N1 cases of different states of USA is available on the website of Centers for Disease Control and Prevention (CDC) (<http://www.cdc.gov/h1n1flu/>), and the data of different provinces of China is available from Sina.com (<http://news.sina.com.cn/z/zhuliugan/>). The data for populations and GDPs of different countries are obtained from English Wikipedia (http://en.wikipedia.org/wiki/List_of_countries_by_population) and (http://en.wikipedia.org/wiki/List_of_countries_by_GDP). There are three different lists of GDPs and what we used here is the one from the World Bank, which includes 182 countries. Among the 135 countries having reported the confirmed H1N1 cases until July 6, 22 of which do not have GDP data. They are all small countries and the number of confirmed cases in these countries is also quite few (the total of the 22 countries are

163 until July 6). We thus ignore them in evaluating the correlation in Fig. 3(c).

0.2 Zipf's Law and Power Law

Zipf's plot is widely used in the statistical analysis of the small-size sample [17], which can be obtained by first rearranging the data by decreasing order and then plotting the value of each data point versus its rank. The famous *Zipf's law* describes a scaling relation, $z(r) \sim r^{-\alpha}$, between the value of data point $z(r)$ and its rank r . As a signature of complex systems, the Zipf's law is widely observed [47, 48]. Indeed, it corresponds to a power-law probability density function $p(z) \sim z^{-\beta}$ with $\beta = 1 + \frac{1}{\alpha}$.

The Heaps' law [6] is another well-known scaling law observed in many complex systems, which describes a sublinear growth of the number of distinct sets $M(t)$ as the increasing of the total number of elements $N_T(t)$ belonging to those sets, with the power-law form $M \sim N_T^\lambda$. Recent empirical analysis [19, 20] suggested that the Heaps' law and Zipf's law usually coexist. Actually, Lü *et al.* [21] proved that if an evolving system has a stable Zipf's exponent, its growth must obey the Heaps' law with exponent $\lambda \approx 1/\alpha$ (an approximate estimation when $\alpha > 1$: the larger the α , the more accurate the estimation).

0.3 Kendall's Tau

In the empirical analysis, the numbers of confirmed cases, populations and GDPs for different countries are very heterogeneous, covering several orders of magnitude (e.g., the population of China is about 2×10^4 times larger than that of Dominica). Thus the classical measurement like the Pearson coefficient is not suitable in analyzing the correlations. We therefore use the rank-based correlation coefficient named *Kendall's Tau*. For two series $\vec{x} = \{x_1, x_2, \dots, x_m\}$ and $\vec{y} = \{y_1, y_2, \dots, y_m\}$, the Kendall's Tau is defined as [49]

$$\tau_K = \frac{2}{m(m-1)} \sum_{i < j} \text{sgn}[(x_i - x_j)(y_i - y_j)], \quad (6)$$

where $\text{sgn}(x)$ is the signum function, which equals +1 if $x > 0$, -1 if $x < 0$, and 0 if $x = 0$. τ_K ranges from +1 (exactly the same ordering of \vec{x} and \vec{y}) to -1 (reverse ordering of \vec{x} and \vec{y}), and two uncorrelated series have $\tau_K \approx 0$.

0.4 On Power-Law Fitting

Most of the distributions P generated by simulations of our model with large β_1 (≥ 0.6) trend to a power-law-like type after several steps of evolution. In the fittings of simulation results, we firstly judge if the curve of P in this range is power-law-like. If yes, we fit the curve by linear function in log-log plots in using least square fit method to get the fitting parameters. The range of the power-law fittings is from 2 to 50. If there is obvious deviation from power-law in this range, we do not use power-law to fit the curve. The only exception is the distribution P when $b = 0.02$ in Fig. 8(a), where the range is from 1 to 30, because the cut-off appears at rank = 30 due to slow spreading of the disease. All the power-law fitting results in the model does not show the error-bar (e.g., the dependence of α on various parameters of the model), because the fitting error on the power-law exponent is far less than the value of α for most cases after 10^4 averages (e.g., $\alpha = 1.666 \pm 0.003$ when $\beta_1 = 0.8$, $\beta_2 = 0.2$, $\rho = 0.2$, $b = 0.06$ and $g = 0.2$ in the minimal model).

0.5 Target Control

When s_i is highly heterogeneous, the nodes with the largest s_i will have the largest number of interregional travels in our model and have high probability to spread the disease. Target control on such nodes may efficiently reduce the spreading. To investigate the impact of the target control, we rank s_i in the

descending order, and put the first R_m nodes in the ranking series as the targets of strong border control. In particular, we take $\beta_1 > 0$ in Eq. (2) for the first R_m nodes with the largest s_i and $\beta_1 = 0$ for the others.

Acknowledgments

References

1. Neumann G, Noda T, Kawaoka Y (2009) Emergence and pandemic potential of swine-origin H1N1 influenza virus. *Nature* 459:931-939.
2. Smith GJD, *et al.* (2009) Origins and evolutionary genomics of the 2009 swine-origin H1N1 influenza A epidemic. *Nature* 459:1122-1126.
3. Rohani P, Breban R, Stallknecht DE, Drake JM (2009) Environmental transmission of low pathogenicity avian influenza viruses and its implications for pathogen invasion. *Proc Natl Acad Sci USA* 106: 10365-10369.
4. Fraser C, *et al.* (2009) Pandemic potential of a strain of Influenza A (H1N1): Early findings. *Science* 324: 1557-1561.
5. Coburn BJ, Wagner BG, Blower S (2009) Modeling influenza epidemics and pandemics: insights into the future of swine flu (H1N1). *BMC Med* 7: 30.
6. Balcan D, *et al.* (2009) Seasonal transmission potential and activity peaks of the new influenza A (H1N1): a Monte Carlo likelihood analysis based on human mobility. *BMC Med* 7: 45.
7. Yang Y, Sugimoto JD, Halloran ME, Basta NE, Chao DL, Matrajt L, Potter G, Kenah E, Longini Jr IM, (2009) The Transmissibility and Control of Pandemic Influenza A (H1N1) Virus. *Science* 326: 729-733.
8. Wallinga J, van Boven M, Lipsitch M. (2010) Optimizing infectious disease interventions during an emerging epidemic. *Proc Natl Acad Sci USA*, 107: 923-928.
9. Hufnagel L, Brockmann D, Geisel T (2004) Forecast and control of epidemics in a globalized world. *Proc Natl Acad Sci USA* 101: 15124-15129.
10. Masuda N, Konno N, Aihara K (2004) Transmission of severe acute respiratory syndrome in dynamical small-world networks. *Phys Rev E* 69: 031917.
11. Small M, Walker DM, Tse CK (2007) Scale-free distribution of avian influenza outbreaks. *Phys Rev Lett* 99: 188702.
12. Colizza V, Barrat A, Barthélemy M, Valleron A-J, Vespignani A (2007) Modeling the Worldwide Spread of Pandemic Influenza: Baseline Case and Containment Interventions. *PLoS Med* 4(1): e13.
13. Ferguson NM, Donnelly CA, Anderson RM (2001) Transmission Intensity and impact of control policies on the foot and mouth epidemic in Great Britain. *Nature* 413: 542-548.
14. Ferguson NM, Donnelly CA, Anderson RM (2001) The Foot-and-Mouth Epidemic in Great Britain: Pattern of Spread and Impact of Interventions. *Science* 292: 1155-1160.

15. Ferguson NM, Cummings DA, Cauchemez S, Fraser C, Riley S, Meeyai A, Iamsirithaworn S, Burke DS (2005) Strategies for containing an emerging influenza pandemic in Southeast Asia. *Nature* 437: 209-214.
16. Longini Jr IM, Nizam A, Xu S, Ungchusak K, Hanshaoworakul W, Cummings DA, Halloran ME (2005) Containing Pandemic Influenza at the Source. *Science* 309: 1083-1087.
17. Zipf GK (1949) *Human Behaviour and the Principle of Least Effort: An introduction to human ecology* (Addison-Wesley, Cambridge).
18. Heaps HS (1978) *Information Retrieval: Computational and Theoretical Aspects* (Academic Press, Orlando).
19. Zhang Z-K, Lü L, Liu J-G, Zhou T (2008) Empirical analysis on a keyword-based semantic system. *Eur Phys J B* 66: 557-561.
20. Cattuto C, Barrat A, Baldassarri A, Schehr G, Loreto V (2009) Collective dynamics of social annotation. *Proc Natl Acad Sci USA* 106: 10511-10515.
21. Lü L, Zhang Z-K, Zhou T (2010) Zipf's law leads to Heaps' law: analyzing their relation in finite-size systems. arXiv:1002.3861.
22. Barthélemy M, Barrat A, Pastor-Satorras R, Vespignani A (2004) Velocity and Hierarchical Spread of Epidemic Outbreaks in Scale-Free Networks. *Phys Rev Lett* 92: 178701.
23. Yang R, Wang BH, Ren J, Bai WJ, Shi ZW, Wang WX, Zhou T (2007) Epidemic spreading on heterogeneous networks with identical infectivity. *Phys Lett A* 364: 189-193.
24. Lipsitch M, et al. (2003) Transmission Dynamics and Control of Severe Acute Respiratory Syndrome. *Science* 300: 1966-1970.
25. Cowling BJ, et al. (2010) Comparative Epidemiology of Pandemic and Seasonal Influenza A in Households. *N Engl J Med* 362: 2175-2184.
26. Cowling BJ, Lau MS, Ho LM, Chuang SK, Tsang T, Liu SH, Leung PY, Lo SV, Lau EH (2010) The effective reproduction number of pandemic influenza: prospective estimation. *Epidemiology* 21:842-846.
27. Nishiura H, Chowell G, Safan M, Castillo-Chavez C (2010) Pros and cons of estimating the reproduction number from early epidemic growth rate of influenza A (H1N1) 2009. *Theoretical Biology and Medical Modelling* 7:1
28. Wu ZL (2004) Scaling Law of SARS onset. *Int J Mod Phys B* 18: 2559-2563.
29. Gross T, D'Lima CJD, Blasius B (2006) Epidemic dynamics on an adaptive network. *Phys Rev Lett* 96: 208701.
30. Han XP (2007) Disease spreading with epidemic alert on small-world networks. *Phys Lett A* 365: 1-5.
31. Moore C, Newman MEJ (2000) Epidemics and percolation in small-world networks. *Phys Rev E* 61: 5678-5682.
32. Newman MEJ (2002) Spread of epidemic disease on networks. *Phys Rev E* 66: 016128.

33. Pastor-Satorras R, Vespignani A (2001) Epidemic spreading in scale-free networks. *Phys Rev Lett* 86: 3200-3203.
34. Moreno Y, Vázquez A (2003) Disease spreading in structured scale-free networks. *Eur. Phys. J. B* 31: 265-271.
35. Gómez-Gardenes J, Latora V, Moreno Y, and Profumo E (2008) Spreading of sexually transmitted diseases in heterosexual populations. *Proc Natl Acad Sci USA* 105: 1399-1404.
36. Pastor-Satorras R, Vespignani A (2002) Immunization of complex networks. *Phys Rev E* 65:036104.
37. Huerta R, Tsimring LS (2002) Contact tracing and epidemics control in social networks. *Phys Rev E* 66: 056115.
38. Cohen R, Havlin S, ben-Avraham D (2003) Efficient immunization strategies for computer networks and populations. *Phys Rev Lett* 91: 247901.
39. Grenfell B, Harwood J (1997) (Meta)population dynamics of infectious diseases. *Trends in Ecol Evol* 12: 395-399.
40. Keeling MJ, Gilligan CA (2000) Metapopulation dynamics of bubonic plague. *Nature* 407:903-906.
41. Fulford GR, Roberts MG, Heesterbeek JAP (2002) The Metapopulation Dynamics of an Infectious Disease: Tuberculosis in Possums. *Theor Pop Biol* 61:15-29.
42. Watt DJ, Muhamad R, Medina DC, Dodds PS (2005) Multiscale, resurgent epidemics in a hierarchical metapopulation model. *Proc Natl Acad Sci USA* 102: 11157-11162.
43. Vergu E, Busson H, Ezanno P (2010) Impact of the Infection Period Distribution on the Epidemic Spread in a Metapopulation Model. *PloS ONE* 5: e9371.
44. Colizza V, Barrat A, Barthélemy M, and Vespignani A (2006) The role of the airline transportation network in the prediction and predictability of global epidemics. *Proc Natl Acad Sci USA* 103: 2015-2019.
45. Balcan D, Colizza V, Gonçalves B, Hu H, Ramasco JJ, and Vespignani A (2009) Multiscale mobility networks and the spatial spreading of infectious diseases. *Proc Natl Acad Sci USA* 106: 21484-21489.
46. Zhang HF, Zhang J, Zhou CS, Small M, and Wang BH (2010) Hub nodes inhibit the outbreak of epidemic under voluntary vaccination. *New J Phys* 12: 023015.
47. Newman MEJ (2005) Power laws, Pareto distributions and Zipf's law. *Contemporary Physics* 46: 323-351.
48. Clauset A, Shalizi CR, Newman MEJ (2009) Power-law distributions in empirical data. *SIAM Rev* 51: 661-703.
49. Kendall M (1938) A New Measure of Rank Correlation. *Biometrika* 30: 81-89.

Table 1. The top 20 countries in the ranking and their total of confirmed cases in five typical dates

Rank	May 1	May 10	May 20	June 10	July 6
1	Mexico 156	U. S. A. 2254	U. S. A. 5469	U. S. A. 13217	U. S. A. 33902
2	U. S. A. 141	Mexico 1626	Mexico 3648	Mexico 5717	Mexico 10262
3	Canada 34	Canada 280	Canada 496	Canada 2446	Canada 7983
4	Spain 13	Spain 93	Japan 210	Chile 1694	U. K. 7447
5	U. K. 8	U. K. 39	Spain 107	Australia 1224	Chile 7376
6	Germany 4	France 12	U. K. 102	U. K. 666	Australia 5298
7	New Zealand 4	Germany 11	Panama 65	Japan 485	Argentina 2485
8	Israel 2	Italy 9	France 15	Spain 331	China 2101
9	Austria 1	Costa Rica 8	Germany 14	Argentina 235	Thailand 2076
10	China 1	Israel 7	Colombia 12	Panama 221	Japan 1790
11	Denmark 1	New Zealand 7	Costa Rica 9	China 166	Philippines 1709
12	Netherlands 1	Brazil 6	Italy 9	Costa Rica 93	New Zealand 1059
13	Switzerland 1	Japan 4	New Zealand 9	Dominican Rep. 91	Singapore 1055
14		Korea, Rep. of 3	Brazil 8	Honduras 89	Peru 916
15		Netherlands 3	China 7	Germany 78	Spain 776
16		Panama 3	Israel 7	France 71	Brazil 737
17		El Salvador 2	El Salvador 6	El Salvador 69	Israel 681
18		Argentina 1	Belgium 5	Peru 64	Germany 505
19		Australia 1	Chile 5	Israel 63	Panama 417
20		Austria 1	Cuba 3	Ecuador 60	Bolivia 416

Tables

Figure Legends

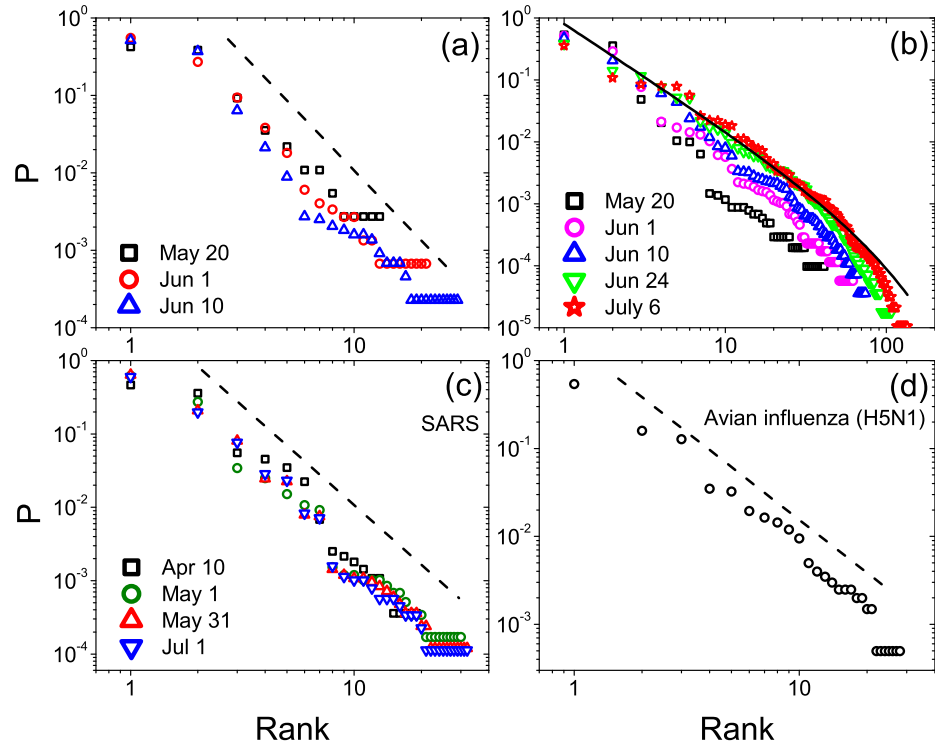


Figure 1. Zipf's distribution of various pandemic diseases. (a) Zipf's distribution of the normalized number of H1N1 cases in different countries in a log-log plot with date before May 15, 2009. (b) Same as (a) but with date after May 15, 2009. (c) Zipf's distribution of the normalized number of probable SARS cases for different countries in 2003. (d) Zipf's distribution of the normalized number of H5N1 cases for different countries in the whole year of 2008. The dash and solid curves are fitting functions described in the text.

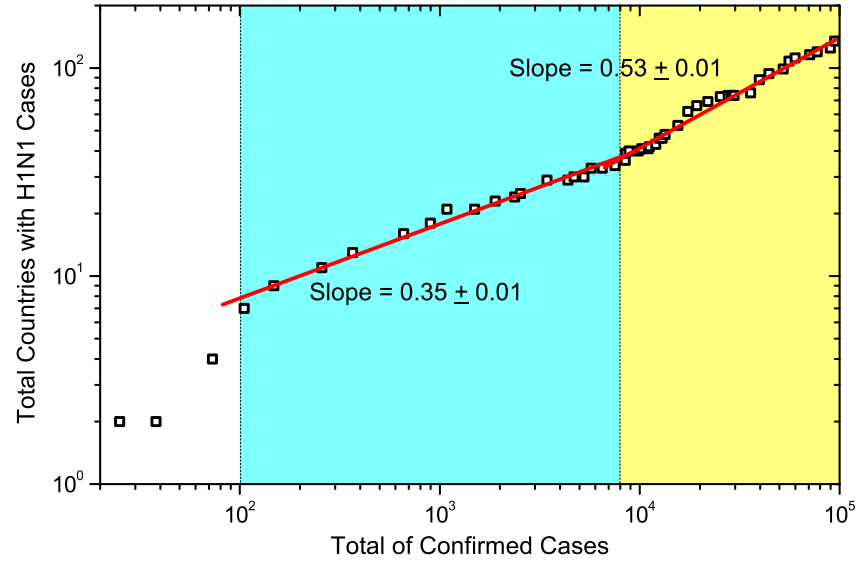


Figure 2. Heaps' law in the spreading of H1N1. Dependence between the number of infected countries, M , and the global total N_T of confirmed cases in log-log plot. The red and yellow areas indicate power-law fitting with slope 0.35 and 0.53, respectively.

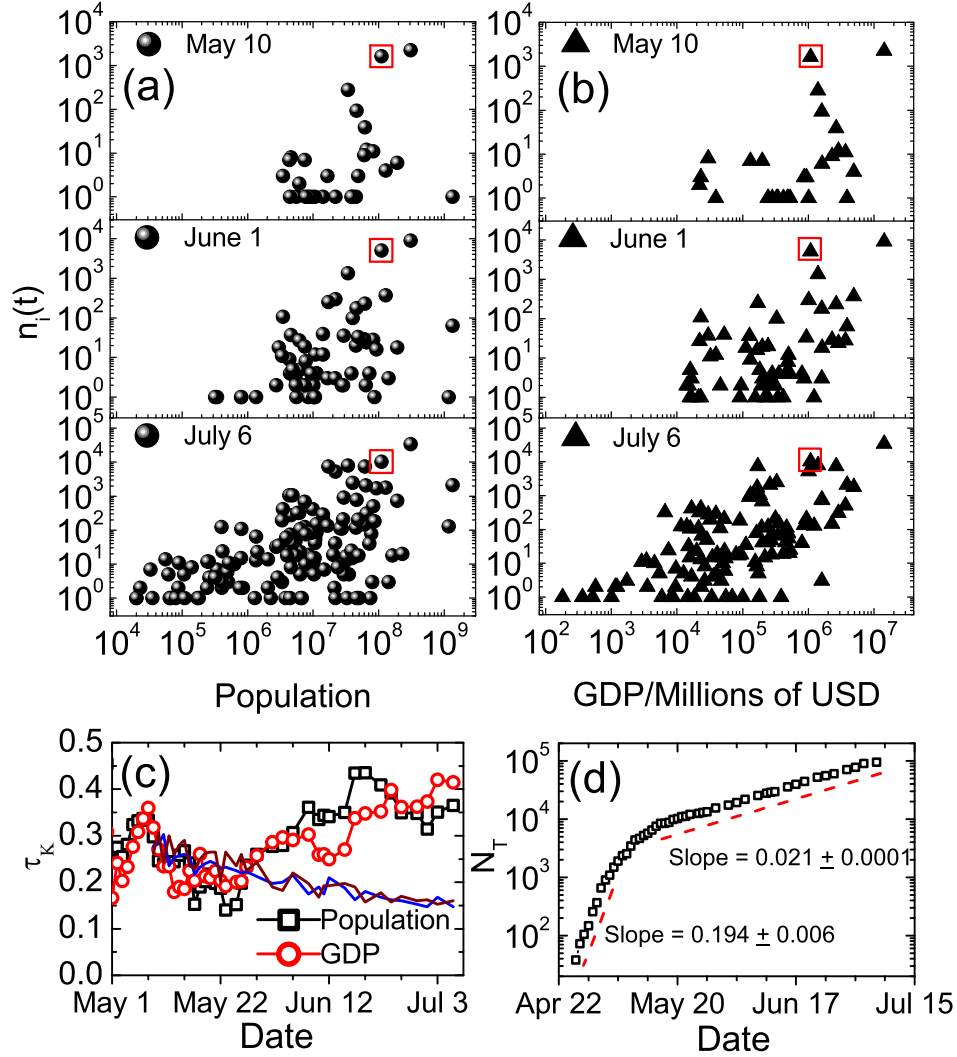


Figure 3. Spreading of H1N1 depends on population and GDP. (a) and (b) show the evolution of the dependence between the number of laboratory-confirmed cases n_i for different countries and the population and GDP of these countries, respectively. The data for Mexico where the disease initiated are highlighted with an open square. (c) The Kendall's Tau τ_K of the correlations between the number of confirmed cases and the population/GDP. After about May 22, τ_K is clearly larger than the 95% significance level (solid red and blue lines) of the surrogate data by randomly shuffling the order of the population/DGP of the countries having reported cases (see *Supporting information*). (d) Growth of global total number N_T of laboratory-confirmed cases of Influenza A in the semi-log plot.

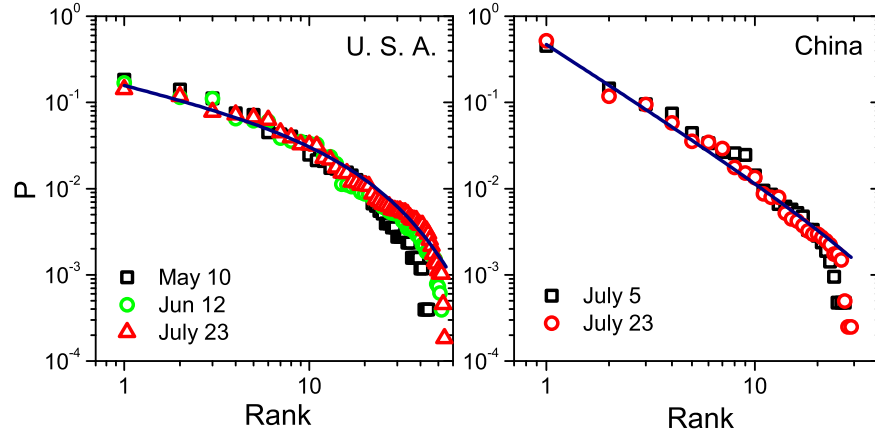


Figure 4. Distribution of epidemic within countries. Normalized distributions P of confirmed cases in different states of USA and different provinces of China. For USA, the solid curve is $P = 0.17r^{-0.51}e^{-0.052r}$, fitting the data of July 23. For China, the solid line is of slope -1.79, fitting the data of July 23.

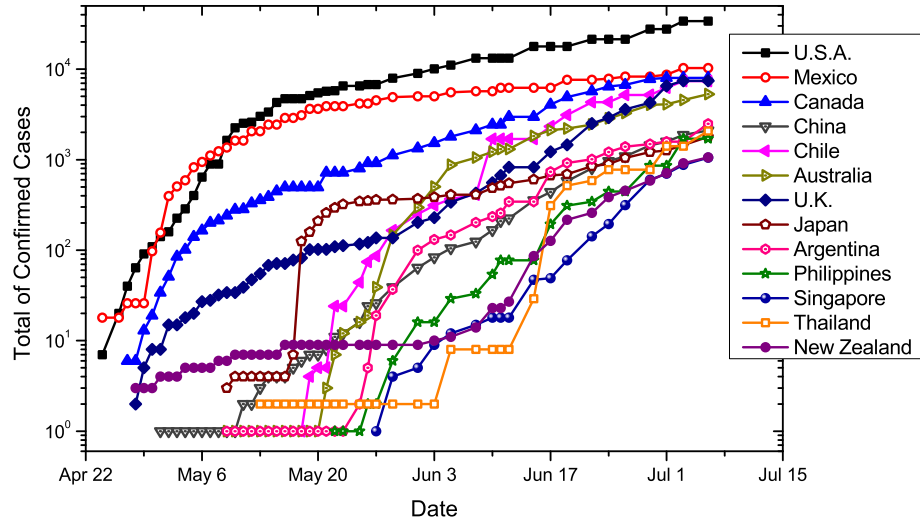


Figure 5. The growth of total confirmed cases within a country.

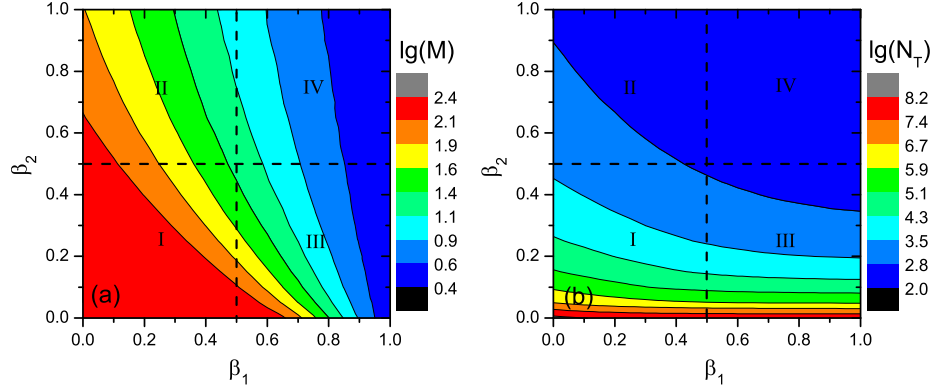


Figure 6. Effects of control on epidemic spreading. Effects of the parameters β_1 and β_2 on spreading speed, measured by the logarithm of the infected range M (a) and the logarithm of the total cases N_T (b) at $t = 100$. Simulations run with $b = 0.06$, and $g = 0.2$, and all the data are averaged over 10^4 independent realizations.

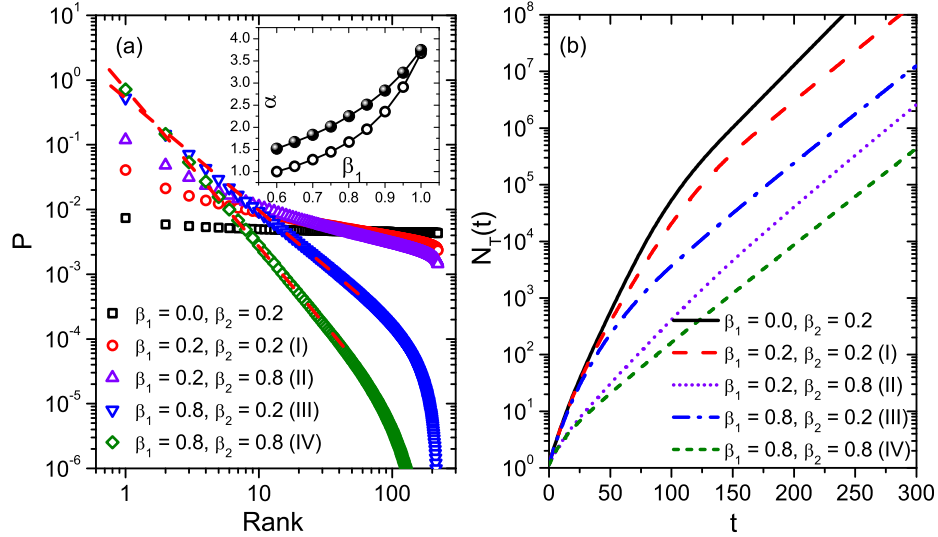


Figure 7. Typical patterns of spreading under various local and interregional control. (a) Typical normalized distribution P (at $t = 300$) in the regime of I, II, III, and IV in the parameter space (β_1, β_2) shown in Fig. 5. The two red dashed lines indicate the power-law functions with $\alpha = 1.67$ and $\alpha = 2.25$, respectively. The inserts show the dependence of α on β_1 for fixed $\beta_2 = 0.2$ (open circle) and $\beta_2 = 0.8$ (filled circle). (b) The corresponding growth of N_T with respect to time. The other parameters are the same as in Fig. 4.

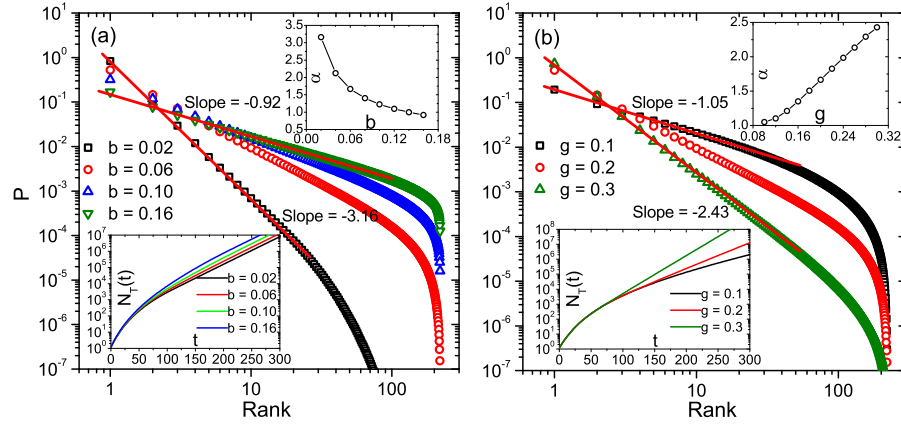


Figure 8. Impacts of b and g on the normalized distributions P . (a) The normalized distributions P for different b . The two red lines are power-law functions with exponent $\alpha = 0.92$ and $\alpha = 3.16$, respectively. The top insert: dependence of α on b . Bottom insert: $N_T(t)$ vs. time for various b . Simulations run with $\beta_1 = 0.8$, $\beta_2 = 0.2$, and $g = 0.2$. (b) The same as (a), but for different g . The two red lines are power-law functions with exponent $\alpha = 1.05$ and $\alpha = 2.43$, respectively. Simulations run with $\beta_1 = 0.8$, $\beta_2 = 0.2$, and $b = 0.06$. All the data are average over 10^4 independent runs.

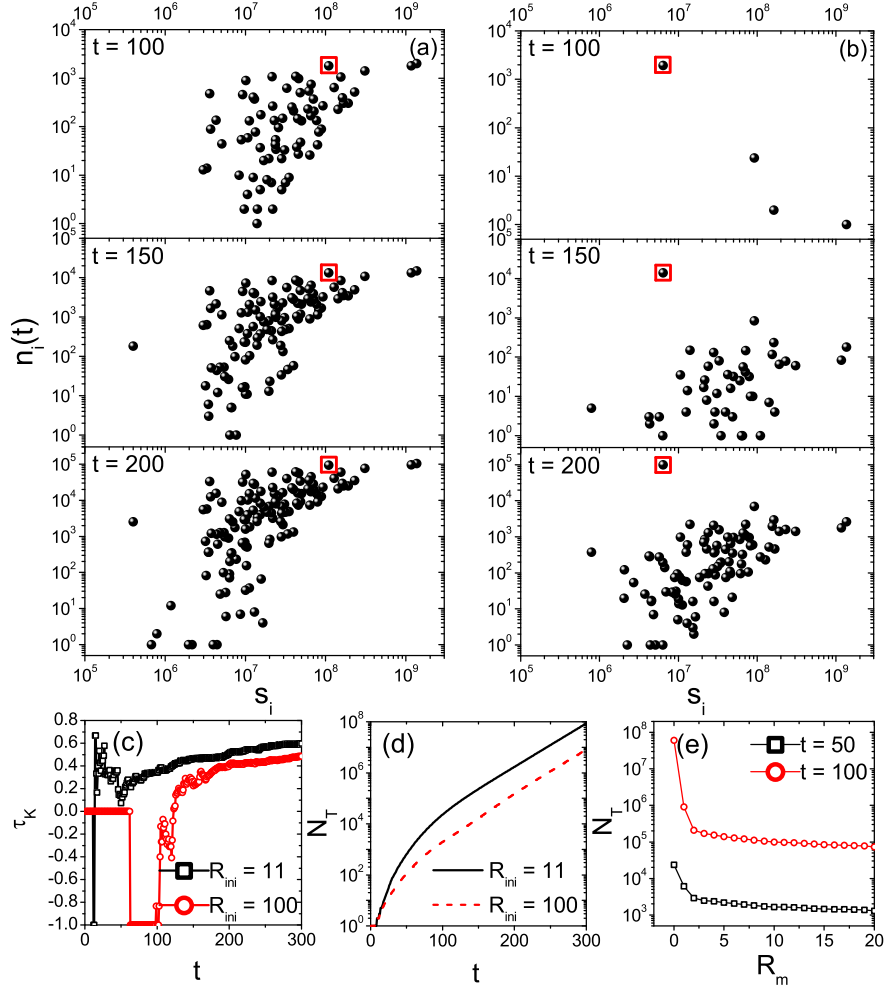


Figure 9. Effects of heterogeneous s_i in the model on epidemic spreading. Here s_i is taken as the population of different countries. (a) and (b) show the evolution of $n_i(t)$ vs s_i when the disease is initiated at different countries (highlighted by an open square). Simulations run with $\beta_1 = 0.8$, $\beta_2 = 0.2$, $b = 0.06$, and $g = 0.2$. (c) Evolution of τ_K between $n_i(t)$ and s_i . (d) The corresponding growth of $N_T(t)$. (a-d) are obtained from one realization of simulation. Statistical results from many realizations are shown in Fig. S7 in SI. (e) N_T at $t = 50$ and $t = 100$ when R_m nodes with the largest s_i are the targets of control with $\beta_1 = 0.8$ (see *Material and Methods*, the other parameters are the same as in (a-d)). Data of (e) are averaged from 10^4 independent runs with disease initiation at random nodes.

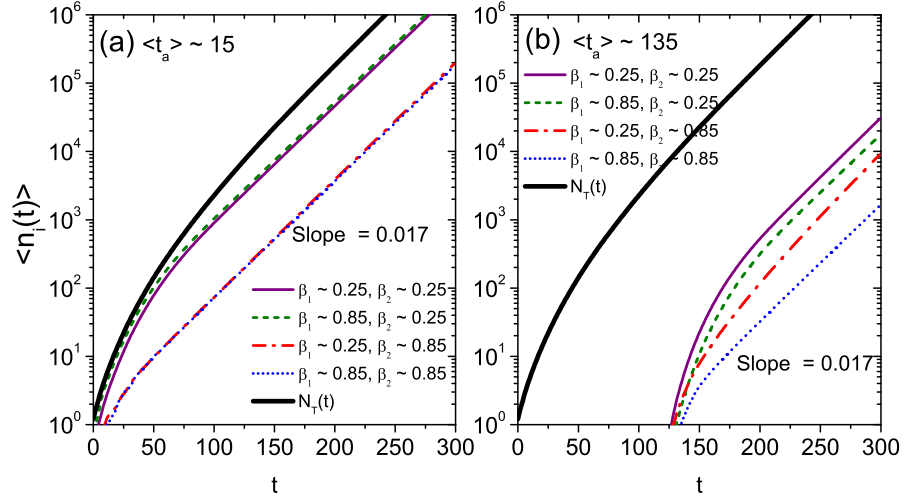


Figure 10. The growth of averaged value of $n_i(t)$ for the nodes with different β_2 , g and the arrival time t_a . (a) For the nodes that $0 \leq t_a < 20$ ($t_a \sim 15$). (b). For the nodes that $130 \leq t_a < 140$ ($t_a \sim 135$). In the two panels, $\beta_1 \sim 0.25$ denotes the data averaged for the nodes that $0.20 \leq \beta_1 < 0.30$, and $\beta_1 \sim 0.85$ for $0.80 \leq \beta_1 < 0.90$, and the same for β_2 . Simulations run with $\rho = 0.2$ and $b = 0.06$ and $g = 0.2$. All the data are average over 10^4 independent runs.

Supporting Information

The robustness of Zipf's distribution

In the surveillance of H1N1 spreading process of each countries, many reasons can lead to the deviation of the reported number of confirmed cases from real number. The ranks of the real number could be different from those of the reported number for some countries. Here we discuss the impact of this deviation on Zipf's plots, and our results show that this impact is slight on the power-law-like distribution of the reported number.

Let us denote the real total number of cases of the i th country as $n'_i = n_i + \varepsilon_i$, where the positive value ε_i represents the error or variation in surveillance of the country. It is reasonable to assume that ε_i could be related to n_i or the population M_i of a country. We consider three types of assumptions on such variation as follows: Type A, the variation is correlated with the reported total of cases, namely $\varepsilon_i = \sigma n_i \eta$, where η is a positive random number and obeys the right-part standard Gaussian distribution; Type B, the variation is correlated with the population of the country, so $\varepsilon_i = \sigma M_i (\frac{\sum_i n_i}{\sum_i M_i}) \eta$, where M_i denotes the population of the country; Type C, the variation is correlated with both the reported total of cases and the population of the country, and we assume $\varepsilon_i = \sigma n_i M_i (\frac{\sum_i n_i}{\sum_i n_i M_i}) \eta$. The terms $\frac{\sum_i n_i}{\sum_i M_i}$ and $\frac{\sum_i n_i}{\sum_i n_i M_i}$ are introduced for the purpose of normalization so that σ value in the three cases are comparable.

The Zipf's distribution of n'_i for these three types of variations are compared to the original distribution in Fig. S1 (a), (b), (c), respectively, for various σ values. While the variation proportional to population (Type B) can result in some deviation of the distribution from the original one, the other two types has no obvious impact on the distribution even though the average variation magnitude σ is large. This result indicate that the power-law-like distribution in Zipf's plot is robust under the variation in Type A and C.

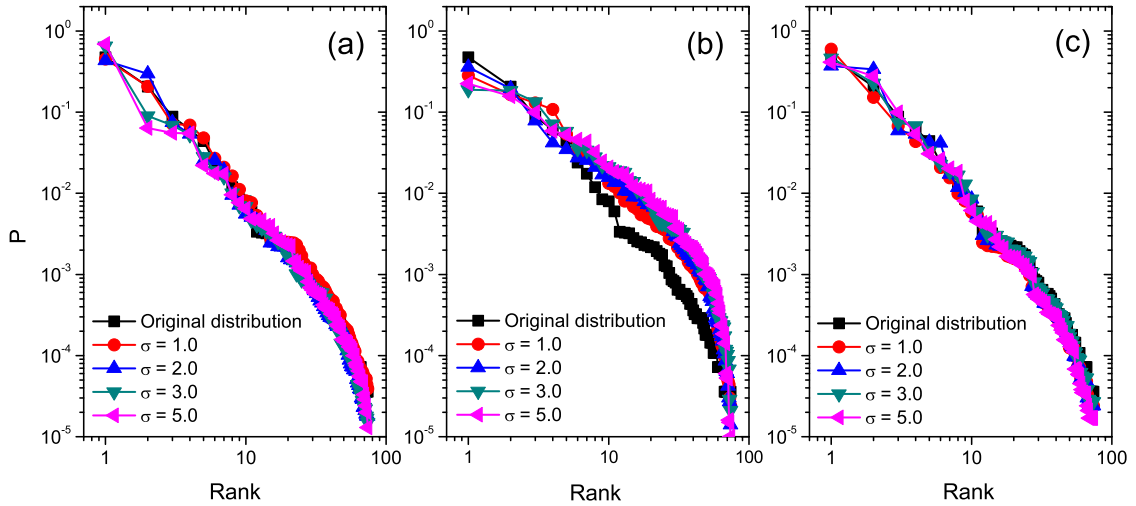


Fig. S1. Comparison of the normalized Zipf's distribution of the three types of variation with different σ to the original distribution of the total of confirmed cases on a typical day (June 10, 2009).

Statistical testing of Kendall's Tau

In this paper, the correlations between the total of confirmed cases of different countries and the populations or GDP of these countries are expressed by the value of Kendall's Tau τ_K . Here we test the significance of τ_K against the finite number of data points.

According to the algorithm of Kendall's Tau, $\tau_K \approx 0$ for two completely uncorrelated serials, however, a non-zero value could be obtained due to the small number of countries with reported cases, especially in the early stage of the spreading. To test the significance of the original τ_K , we compare it to τ'_K from surrogate data where the series of the population or GDP of the corresponding countries is randomly shuffled. We can obtain a distribution of τ'_K for the surrogate for many realizations, and such a distribution is normal-like around $\tau'_K = 0$. From this distribution, we can obtain the 95% significance levels. If the original τ_K is out of these levels, then there is less than 5% of possibility that the original τ_K is due to coincidence in finite size uncorrelated series. Note that, in the early stage of May, there are just very few countries with reported cases. The number of shuffling realizations in the surrogate data is too small to obtain a reliable distribution of τ'_K .

Fig. S2 shows the comparison between τ_K and the distribution of τ'_K . While in the early stage (before May 22) we cannot reject the null hypothesis with very high confidence that the two series are uncorrelated, τ_K is clearly significant afterwards for both the population and GDP.

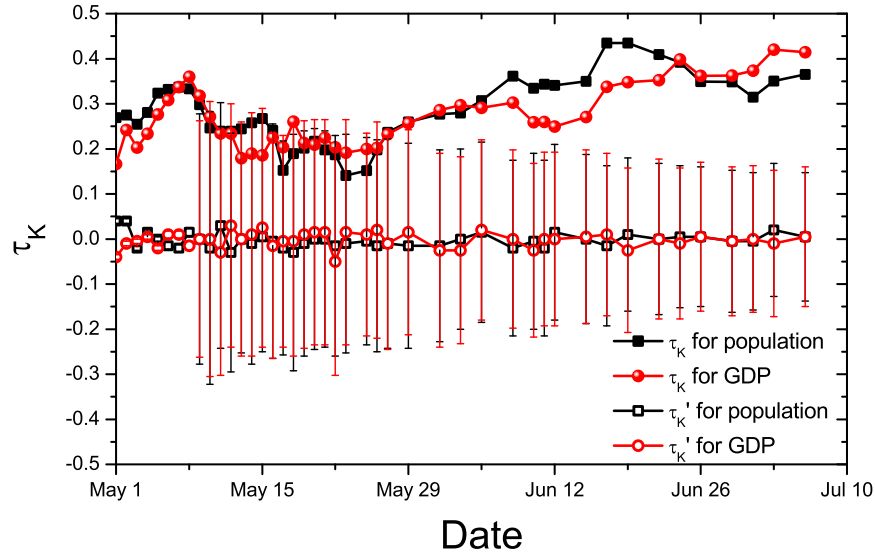


Fig. S2. Testing significance of Kendall's Tau that measures the correlations between total of confirmed cases and population / GDP of each of the countries. The range of error-bar denotes 95% of the significance level. Since the number of countries with reported cases is few in the early stage of May, the error-bars are absent.

Estimation of the reproductive number R in global level

As shown in the main text (Fig. 3(d)), the growth of the global total of confirmed cases after the middle of May can be well fitted by a straight line with a slope 0.021 in semi-log plots, namely, the growth follows

a stable exponent form $\exp(\lambda t)$ with a daily rate, $\lambda = 0.021 \times \ln(10) = 0.048$. In our estimation of the reproductive number R , we assumed that all the population is susceptible, and thus $R = R_0$, where R_0 is the basic reproductive number. We used the formula in Ref. [1], $R = 1 + V\lambda + f(1-f)(V\lambda)^2$, where f is the ratio of the infectious period to the serial interval, and V is the mean serial interval, the sum of the mean infectious and mean latent periods. According to Ref. [2, 3], the serial interval was estimated to be in a range with mean 3.2 days and standard deviation 1.3 days. Therefore, the range of the serial interval V is set between 1.9 and 4.5 in our estimation. Assuming $f = 0.7$ or 0.3 [1], the reproductive number R changes from 1.09 to 1.22 when V increases 1.9 days to 4.5 days (Insert in Fig. S3). This range of R value is slightly less than the ranges obtained in several other researches based on the early period [4, 5], but in agreement with the results obtained from the data in the summer of 2009 [3].

We also investigated the evolution of the reproductive number R in the pandemic Influenza A (H1N1) (Fig. S3 (a)). The daily growth rate λ are obtained from the growth of total of confirmed cases in each two or three days. The estimated value of R is higher than 4 in the last a few days in April and then sharply reduces to a normal value between 1.0 and 1.4 after the middle of May. This reduction of R may reflects the effect of various control and intervention schemes.

Interestingly, the evolution of the estimated reproduction number R is related to the Zipf's distribution P . As seen in Fig. S3(b), during the period when R sharply reduces (before the middle of May), the exponent α of P keeps in a higher level between 2.8 and 3.7. From the middle of May to July, α steadily declines from higher than 3 to 1.7 while R trends to stable. R and α appear to be positively correlated in the early stage of pandemic (insert in Fig. S3(b)).

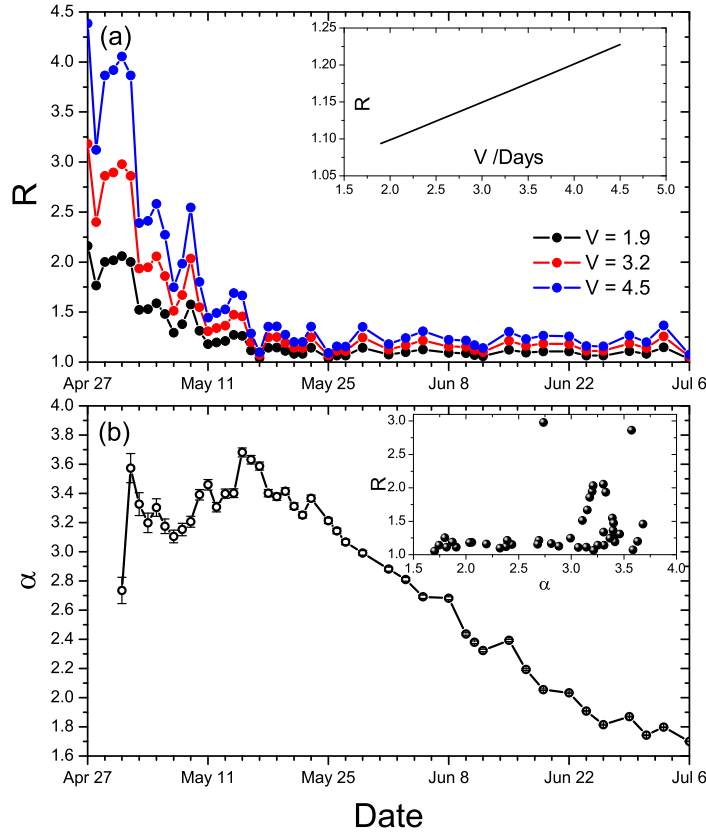


Fig. S3. (a) Time evolution of the estimated reproduction number R from April 28 to July 6. The insert shows

R (of a given date) for different serial intervals V from 1.9 days to 4.5 days. (b) Time evolution of the power-law exponent α of the normalized distribution P of the total of confirmed cases, and the insert shows possible positive correlation R and α when both of them are large in the early stage.

Evolution of the reproductive number R in our model

The evolution of the reproductive number R estimated from the growth of N_T in our model is compared with R estimated from real data. For the comparison, the time scale in our model is rescaled by the following method: Firstly, we find two times t_1 and t_2 in the growth curve of N_T in the model to satisfy $N_T(t_1) \approx 38$ and $N_T(t_2) \approx 94512$. The numbers 38 and 94512 are the global total of confirmed cases in April 26 and July 6, respectively. There are 71 days from April 26 to July 6, thus we assume the length of one time step in our model is corresponding to $\frac{71}{t_2 - t_1}$ days. Consequently, the growth rate of each time step in our model is $\lambda(t) = [\ln(N_T(t)) - \ln(N_T(t_1))](t_2 - t_1)/71$. From the growth rate $\lambda(t)$, the reproductive number $R(t)$ can be obtained as in the real data. As shown in Fig. S4, in our typical parameter settings ($\beta_1 = 0.8$, $\beta_2 = 0.2$, $b = 0.06$ and $g = 0.2$), the evolution of R also shows a rapid decrease: R changes from the range between 1.7 and 3.0 to the range between 1.1 and 1.4, and generally in agreement with our empirical estimation of R .

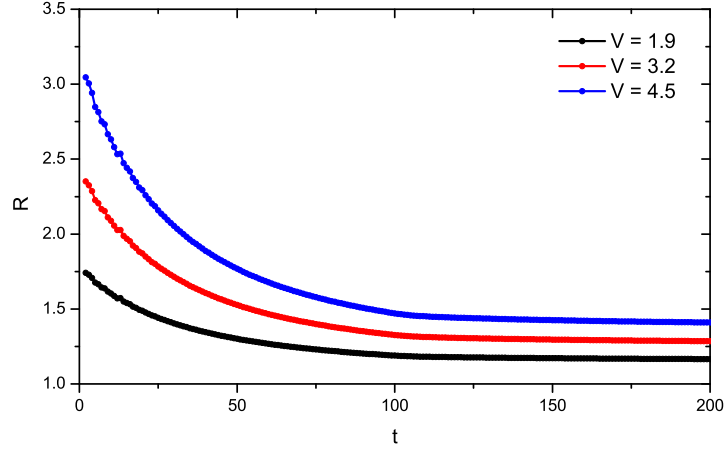


Fig. S4. Time evolution of the reproduction number R estimated from the model simulation result. Parameter settings are $\beta_1 = 0.8$, $\beta_2 = 0.2$, $b = 0.06$ and $g = 0.2$.

The evolution of Zipf's distribution P vs. the Heaps' plots in the model

The empirical results in Fig. 1(b) in the paper indicates that the Zipf's plot converges to a stable distribution before the range of spreading M reaches saturation. The convergence to a stable distribution is inherent in our model. Let us consider a few nodes in the model with the largest n_i . The growth n_i in such nodes is mainly determined by the local growth rate ρg , $n_i(t+1) \approx (1 + \rho g)n_i(t)$, since the

number of infected case due to input from other nodes is much smaller and can be neglected and the local growth has shifted to a stable rate due to local control in Eq. 4. When considering a power-law Zipf's distribution at time t , $P_t(r) \sim r^{-\alpha}$, the total global cases N_T are mainly contributed by these nodes with the largest n_i , i.e., $N_T(t+1) \approx (1 + \rho g)N_T(t)$. Thus the normalized distribution at $t+1$ for these nodes is $P_{t+1}(r) = n_i(t+1)/N_T(t+1) \approx n_i(t)/N_T(t) \sim r^{-\alpha}$ which is invariant vs. time. This analysis is confirmed by the evolution of P at various parameters in Fig. S5(a-d). We can see that the distributions P at different time overlap for the nodes with the smallest ranks r . The range of the forepart of the curve of P which can be well fitted by power-law extends along with the time evolution, and the cut-off tail will move to large ranks r till it reaches the system size K .

In our model, the scaling property in the distribution P is mainly contributed by large β_1 . An extreme situation is that $\beta_1 > 0$ and $\beta_2 = 0$, namely, the effect of local control is ignored (the parameter g does not have any impacts). In this case, $n_i(t+1) \approx (1 + \rho)n_i(t)$ for the nodes with the largest n_i and $N_T(t+1) \approx (1 + \rho)N_T(t)$. P converges quickly to a power-law distribution when β_1 is large (Fig. S5(a)), and the exponent α is quite large because n_i of early infected nodes grow very fast, leading to a heterogeneous distribution. On the other hand when β_2 is large enough, the growth of n_i and N_T will shift quickly to a stable rate ρg and P again converges to a power-law distribution. α is significantly smaller than that at $\beta_2 = 0$ because the local control reduces significantly the growth rate of the early infected nodes, and n_i is not as heterogeneous. The stronger the control, the slower the growth of the newly infected nodes, and the more heterogeneous the distribution. Therefore, the convergent exponent α becomes larger when β_2 increases. When β_2 is small, it takes a long period of time for infected nodes to achieve an stable exponential growth and consequently it takes many steps for P to converge.

In the discussions of the results of our model, the evolution time of the model generally is set as 300 steps, because in the parameter settings in our discussion, most of the P distributions can show long range of power-law part and the exponent of the power-law part trends to stable after 300 steps of evolution.

From Fig. S5(a-d) we can also see that the distribution at a given time t has a cut-off at the range of spreading, i.e. $r = M(t)$. At this point, we have $P(r) \approx 1/N_T(t)$ the last infect countries usually just has one or a few cases. When α is large (e.g., Fig. S5(a)), as an approximation we can assume that the power-law distribution $P(r) \sim r^{-\alpha}$ extends to the cut-off point, i.e., $P(r) \approx 1/N_T(t) \sim M^{-\alpha}(t)$; and we get $M \sim N_T^{\lambda}$ where $\lambda = 1/\alpha$, implying that the Heaps' law [6] can be observed in the process (similar analysis could be found in [7], while for more accurate estimation, please see Ref. [8]). The Heaps' plots corresponding to the Zipf's plots in Fig. S5(a-d) are shown in Fig. S5(e-g). We can see that the fitting exponents satisfy $\lambda\alpha \approx 1$ as expected from the analysis. The Heaps' plots also manifest the saturation of M when N_T becomes very large.

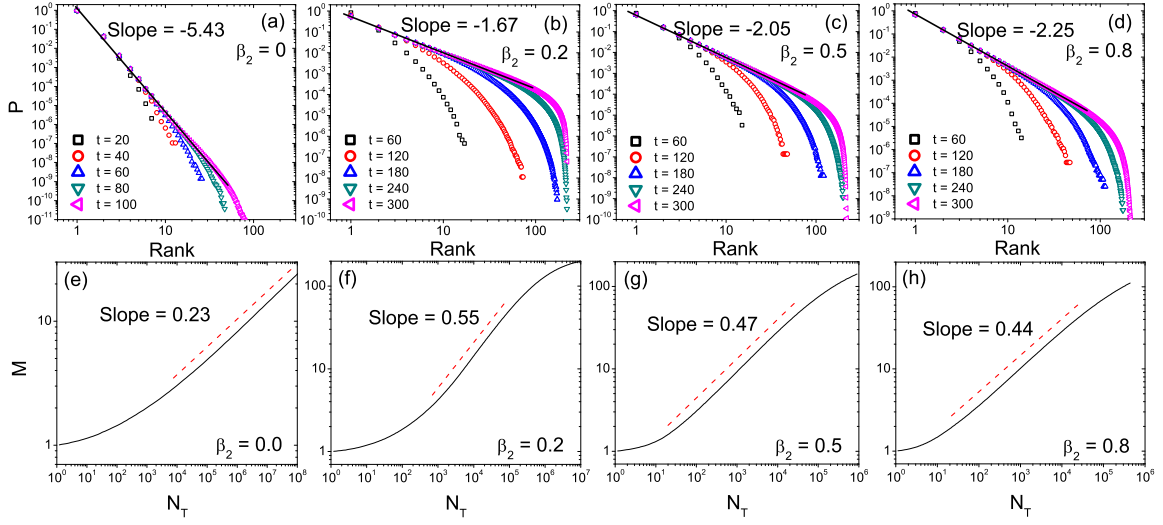


Fig. S5. Upper panel (a-d): Evolution of the normalized Zipf's distributions P at different time steps of the model for various β_2 . The other parameters are $\beta_1 = 0.8$, $b = 0.06$, $\rho = 0.2$ and $g = 0.2$. All the data are average over 10^4 independent runs. Lower panel (e-h): Dependence between M and N_T (Heaps' plot) generated by the model for different β_2 , corresponding to the distributions P shown in (a)-(d), respectively.

Effects of heterogeneity in s_i

In the paper we discuss the effect of heterogeneity in s_i by taking s_i as the population of a country. Fig. 9 in the paper shows the evolution of the dependence between $n_i(t)$ and s_i in one realization of the model simulation when the disease is initiated at two countries with population rank $R_{ini} = 11$ and $R_{ini} = 100$, respectively. Fig. S6 displays the statistics over many realizations: (a) and (b) show the probability density function in the space $(\log_{10} s_i, \log_{10} n_i)$ with color scale and (c) and (d) are the time evolution of the total cases N_T and the Kendall's Tau, corresponding to Fig. 9 in the paper. In the early stage, the initiation position is the center of spreading, but shortly, the nodes with the largest s_i become the super-spreaders. The spreading from the nodes with large s_i to those with small s_i becomes very evident in this presentation.

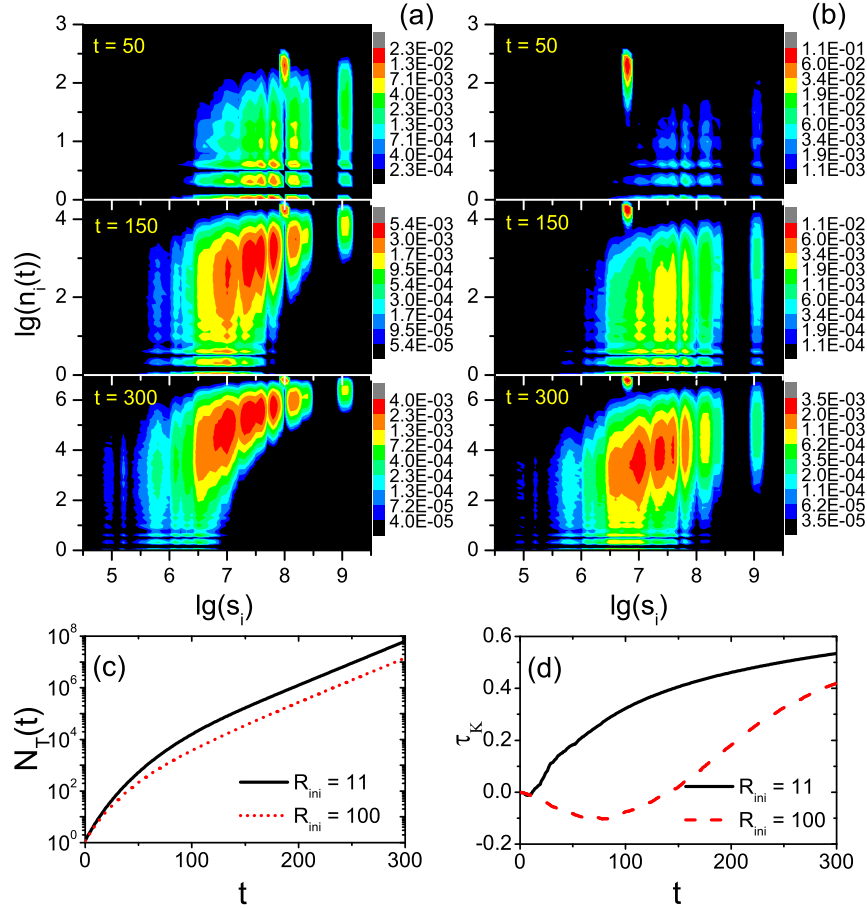


Fig. S6. Evolutions of the probability density in the space $(\log_{10} s_i, \log_{10} n_i)$ obtained from 10^4 realizations of simulations with the epidemic initiation at node with population rank $R_{ini} = 11$ (a) and $R_{ini} = 100$ (b). The corresponding growth of $N_T(t)$ (c) and evolution of Kendall's Tau τ_K between $n_i(t)$ and s_i (d) averaged over all the realizations. Simulations run on $\beta_1 = 0.8$, $\rho = 0.2$, $b = 0.06$, and $g = 0.2$.

In the following we carry out a more systematic analysis of the impact of heterogeneous s_i and target control by considering power distributions of s_i , i.e., $P(s) \sim s^{-\gamma}$. Two spreading processes are compared. The first one is the situation without any control impacts, namely $\beta_1 = 0$ and $\beta_2 = 0$. In the second situation we consider strong border control ($\beta_1 = 0.8$ and $\beta_2 = 0.2$, typical parameter setting introduced in Fig. 7 in the paper).

Without control, the spreading is very fast even in the case of uniform s_i . Simulation results indicate that increased heterogeneity at smaller γ sharply accelerates the spreading by increasing the total cases N_T in all the spreading period (Fig. S7(a)). The impact of heterogeneity on the spreading range M varies in different periods of the spreading: for stronger heterogeneity (smaller γ), M is larger in the early stage, but smaller in the later stages (Fig. S7(b)). With control, the spreading is significantly suppressed (e.g., compare $t = 100$ in panel (c) to $t = 60$ in panel (a)), and the acceleration by the heterogeneity is weaker: N_T does not increase so strongly when γ is smaller (Fig. S7(c)), while M displays similarly non-monotonic but relatively stronger dependence on γ (Fig. S7(d)). The non-monotonic impact of heterogeneity on M

can be understood as follows. When s_i become rather heterogeneous, the epidemic will rapidly arrive at the nodes with large s_i when initiated at a random node (see Fig. S7(b)), so M is larger at smaller γ in the early stage. Then the epidemic mainly grows in these a few early infected nodes with the largest s_i and the majority of nodes with small s_i have rather weak connections between them, which makes the spreading to new nodes more difficult, even though the total cases N_T is larger. In the situations with control, the spreading from these nodes having the largest s_i and n_i to the nodes with small s_i is further reduced. As a result, the non-monotonic impact on M is more obvious in the situations with control. The enhanced spreading by the heterogeneity, however, only makes the distribution P slightly more homogeneous (Fig. S8).

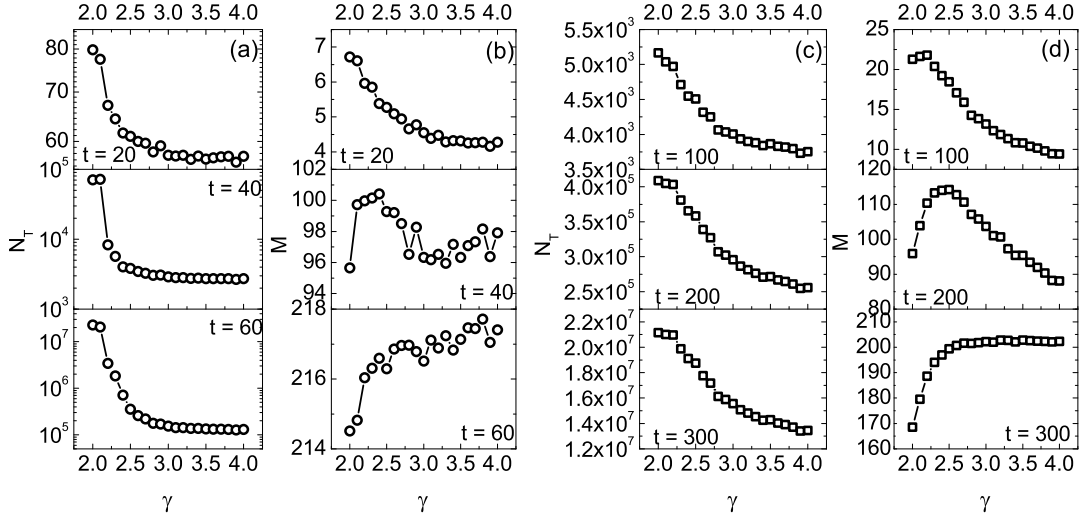


Fig. S7. Impacts of node heterogeneity (γ) on the total cases N_T and range M of the epidemic spreading without control (panels (a) and (b): $\beta_1 = 0$ and $\beta_2 = 0$) and with control (panels (c) and (d): $\beta_1 = 0.8$ and $\beta_2 = 0.2$). Note the different scales in the y-axes of (a) and (c). The simulations run on $\rho = 0.2$, $b = 0.06$, and $g = 0.2$. All of data are averaged from 10^4 independent runs.

The comparison of these heterogeneous networks with the minimal models show that while strong heterogeneity in the nodes (countries) could be an accelerating factor, just like the effect of the heterogeneous degree distribution of complex networks [9], the strengths of control play a leading and dominant role in determining the epidemic spreading patterns. In fact, the impact of strong heterogeneity can be compensated with slightly increased border control parameter β_1 .

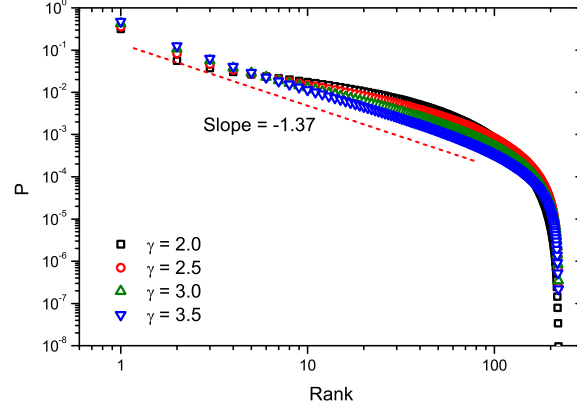


Fig. S8. The distributions P for different γ at $t = 300$. Simulation runs on $\beta_1 = 0.8$, $\beta_2 = 0.2$, $\rho = 0.2$, $b = 0.06$, and $g = 0.2$. The red dashed line denotes the power-law with exponent -1.37 . All of data are obtained at $t = 300$ and averaged from 10^4 independent runs.

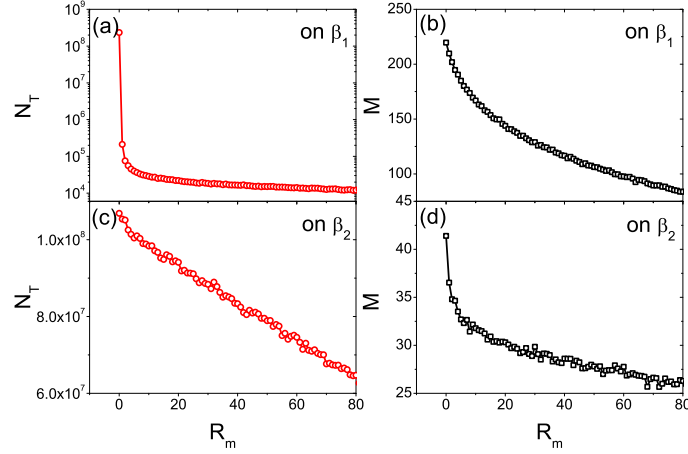


Fig. S9. (a) and (b): Total cases N_T and range M vs. R_m , the number of nodes with target border control ($\beta_1 = 0.8$ for the R_m nodes with the largest s_i , and $\beta_1 = 0$ for others). Simulations run on $\gamma = 2.0$, $\beta_2 = 0.2$, $\rho = 0.2$, $b = 0.06$, and $g = 0.2$. (c) and (d): as in (a) and (b), but with target local control ($\beta_2 = 0.2$ for the R_m nodes with the largest s_i , and $\beta_2 = 0$ for others). Simulations run on $\gamma = 2.0$, $\beta_1 = 0.8$, $\rho = 0.2$, $b = 0.06$. All of data are obtained at $t = 100$ and averaged from 10^4 independent runs.

Generally speaking, the nodes with large intensity on heterogeneous structures usually are the keys towards the dynamics of the system. We have applied the target control to the first R_m nodes with the largest s_i . The spreading can be sharply decelerated by reducing both the total cases N_T and range M (Fig. S9(a) and (b)), when only a few nodes with the largest s_i are in strong border control (setting $\beta_1 > 0$ for the first R_m nodes and $\beta_1 = 0$ for the others). Similar impact can also be observed with target local control on the same nodes (setting $\beta_2 > 0$ for the front R_m nodes and $\beta_2 = 0$ for others, see

Fig. S9(c) and (d)). In this case, infection in those nodes with $\beta_2 = 0$ grows very fast (with a rate ρ) and the control on a few nodes does not reduce the total N_T very significantly. However, M is clearly reduced because the nodes with the largest s_i are usually the centers of spreading in the early stage and the target control within these nodes will retard the spreading to other nodes. These impacts of control on the nodes with large s_i are quite similar to the targeted immunization strategy on hubs nodes with the largest degrees in scale-free networks [10]. Therefore, the heterogeneity could be employed to prevent the spreading with target control strategies, and the target control over a few nodes can save the overall cost of control.

References

1. Lipsitch M, *et al.* (2003) Transmission dynamics and control of Severe Acute Respiratory Syndrome. *Science* 300: 1966-1970.
2. Cowling BJ, *et al.* (2010) Comparative Epidemiology of Pandemic and Seasonal Influenza A in Households. *N Engl J Med* 362: 2175-2184.
3. Cowling BJ, Lau MS, Ho LM, Chuang SK, Tsang T, Liu SH, Leung PY, Lo SV, Lau EH (2010) The effective reproduction number of pandemic influenza: prospective estimation. *Epidemiology* 21:842-846.
4. Fraser C, *et al.* (2009) Pandemic potential of a strain of Influenza A (H1N1): Early findings. *Science* 324: 1557-1561.
5. Nishiura H, *et al.* (2010) Pros and cons of estimating the reproduction number from early epidemic growth rate of influenza A (H1N1) 2009. *Theoretical Biology and Medical Modelling* 7:1.
6. Heaps HS (1978) *Information Retrieval: Computational and Theoretical Aspects* (Academic Press, Orlando).
7. Baeza-Yates RA, Navarro G (2000) Block addressing indices for approximate text retrieval. *J. Am Soc Inf Sci* 51: 69-82.
8. Lü L, Zhang Z-K, Zhou T (2009) Zipf's law leads to Heaps' law: analyzing their relation in finite-size systems . unpublished.
9. Pastor-Satorras R, Vespignani A (2001) Epidemic spreading in scale-free networks. *Phys Rev Lett* 86: 3200-3203.
10. Pastor-Satorras R, Vespignani A (2002) Immunization of complex networks. *Phys Rev E* 65:036104.

Table 2. Rank of total of confirmed cases for different countries (I)

Rank	May 1	May 10	May 20	June 10	July 6
1	Mexico 156	U. S. A. 2254	U. S. A. 5469	U. S. A. 13217	U. S. A. 33902
2	U. S. A. 141	Mexico 1626	Mexico 3648	Mexico 5717	Mexico 10262
3	Canada 34	Canada 280	Canada 496	Canada 2446	Canada 7983
4	Spain 13	Spain 93	Japan 210	Chile 1694	U. K. 7447
5	U. K. 8	U. K. 39	Spain 107	Australia 1224	Chile 7376
6	Germany 4	France 12	U. K. 102	U. K. 666	Australia 5298
7	New Zealand 4	Germany 11	Panama 65	Japan 485	Argentina 2485
8	Israel 2	Italy 9	France 15	Spain 331	China 2101
9	Austria 1	Costa Rica 8	Germany 14	Argentina 235	Thailand 2076
10	China 1	Israel 7	Colombia 12	Panama 221	Japan 1790
11	Denmark 1	New Zealand 7	Costa Rica 9	China 166	Philippines 1709
12	Netherlands 1	Brazil 6	Italy 9	Costa Rica 93	New Zealand 1059
13	Switzerland 1	Japan 4	New Zealand 9	Dominican Rep. 91	Singapore 1055
14		Korea, Rep. of 3	Brazil 8	Honduras 89	Peru 916
15		Netherlands 3	China 7	Germany 78	Spain 776
16		Panama 3	Israel 7	France 71	Brazil 737
17		El Salvador 2	El Salvador 6	El Salvador 69	Israel 681
18		Argentina 1	Belgium 5	Peru 64	Germany 505
19		Australia 1	Chile 5	Israel 63	Panama 417
20		Austria 1	Cuba 3	Ecuador 60	Bolivia 416
21		China 1	Guatemala 3	Guatemala 60	Nicaragua 321
22		Colombia 1	Korea, Rep. of 3	Philippines 54	El Salvador 319
23		Denmark 1	Netherlands 3	Italy 50	France 310
24		Guatemala 1	Peru 3	Korea, Rep. of 48	Guatemala 286
25		Ireland 1	Sweden 3	Brazil 36	Costa Rica 277
26		Poland 1	Finland 2	Colombia 35	Venezuela 206
27		Portugal 1	Malaysia 2	Nicaragua 29	Ecuador 204
28		Sweden 1	Norway 2	Uruguay 24	Korea, Rep. of 202
29		Switzerland 1	Poland 2	New Zealand 23	Uruguay 195
30			Thailand 2	Netherlands 22	Viet Nam 181
31			Turkey 2	Kuwait 18	Greece 151
32			Argentina 1	Singapore 18	Italy 146
33			Australia 1	Paraguay 16	Netherlands 135
34			Austria 1	Sweden 16	India 129
35			Denmark 1	Switzerland 16	Brunei Darussalam 124
36			Ecuador 1	Viet Nam 15	Honduras 123
37			Greece 1	Belgium 14	Colombia 118
38			India 1	Ireland 12	Saudi Arabia 114
39			Ireland 1	Venezuela 12	Malaysia 112
40			Portugal 1	Turkey 10	Cyprus 109
41			Switzerland 1	Norway 9	Dominican Rep. 108
42				Romania 9	Paraguay 106
43				Denmark 8	Cuba 85
44				Egypt 8	Sweden 84
45				Lebanon 8	Egypt 78
46				Thailand 8	Switzerland 76
47				Jamaica 7	Ireland 74
48				Poland 6	Denmark 66
49				Austria 5	Trinidad and Tobago 65
50				Cuba 5	West Bank and Gaza Strip 60
51				Greece 5	Belgium 54
52				Malaysia 5	Lebanon 49
53				Estonia 4	Finland 47
54				Finland 4	Portugal 42
55				India 4	Norway 41
56				Bolivia 3	Romania 41
57				Hungary 3	Turkey 40
58				Russia 3	Kuwait 35
59				Slovakia 3	Jamaica 32
60				Bahamas 2	Poland 25
61				Barbados 2	Malta 24
62				Bulgaria 2	Jordan 23
63				Czech Republic 2	Qatar 23
64				Iceland 2	Indonesia 20
65				Portugal 2	Austria 19
66				Trinidad and Tobago 2	Sri Lanka 19
67				Bahrain 1	Bangladesh 18
68				Cayman Islands, UKOT 1	Slovakia 18
69				Cyprus 1	South Africa 18
70				Dominica 1	USA Puerto Rico 18
71				Luxembourg 1	Morocco 17
72				Saudi Arabia 1	Bahrain 15
73				Ukraine 1	Czech Republic 15
74				United Arab Emirates 1	Kenya 15
75					Serbia 15
76					Cayman Islands, UKOT 14
77					Slovenia 14
78					Estonia 13
79					Barbados 12
80					France, New Caledonia, FOC 12
81					Iraq 12
82					Hungary 11
83					Suriname 11
84					U. K., Jersey, Crown Dependency 11
85					Bulgaria 10
86					Montenegro 10
87					Netherlands Antilles, Curaao * 8
88					United Arab Emirates 8
89					Yemen 8
90					Bahamas 7

Table 3. Rank of total of confirmed cases for different countries (II)

Rank	May 1	May 10	May 20	June 10	July 6
91					Cambodia 7
92					Netherlands Antilles, Sint Maarten 7
93					Luxembourg 6
94					Algeria 5
95					Laos 5
96					Nepal 5
97					Netherlands, Aruba 5
98					Tunisia 5
99					U. K., Guernsey, Crown Dependency 5
100					France, French Polynesia, FOC 4
101					Iceland 4
102					Oman 4
103					Cap Verde 3
104					Ethiopia 3
105					France, Martinique, FOC 3
106					Lithuania 3
107					Russia 3
108					Antigua and Barbuda 2
109					British Virgin Islands, UKOT 2
110					Cote d'Ivoire 2
111					Fiji 2
112					France, Guadeloupe, FOC 2
113					Guyana 2
114					The former Yugoslav Rep. of Macedonia 2
115					Vanuatu 2
116					Bermuda, UKOT 1
117					Bosnia and Herzegovina 1
118					Cook Island 1
119					Croatia 1
120					Dominica 1
121					France Saint Martin, FOC 1
122					Iran 1
123					Latvia 1
124					Libya 1
125					Mauritius 1
126					Myanmar (Burma) 1
127					Palau 1
128					Papua New Guinea 1
129					Saint Lucia 1
130					Samoa 1
131					Syria 1
132					Uganda 1
133					Ukraine 1
134					U. K., Isle of Man, Crown Dependency 1
135					USA Virgin Islands 1
Total:	367	4379	10243	27737	94512